DIFFUSION INTERACTIONS IN

COPPER - ZINC -

TIN ALLOYS

DIFFUSION INTERACTIONS IN COPPER - RICH COPPER - ZINC - TIN ALLOYS

By

ROBERT J. BRIGHAM, B.Sc.

A Thesis

Submitted to the Faculty of Graduate Studies

in Partial Fulfilment of the Requirements

for the Degree

Master of Science

McMaster University

September 1963

MASTER OF SCIENCE (1963) McMASTER UNIVERSITY
(Metallurgy) Hamilton, Ontario.

TITLE: Diffusion Interactions in Copper-rich Copper-Zinc-Tin Alloys.

AUTHOR: Robert John Brigham, B.Sc. (McMaster University)

SUPERVISOR: Professor J.S. Kirkaldy

NUMBER OF PAGES: v, 49

SCOPE AND CONTENTS:

In this thesis, an investigation of various diffusion couple designs is discussed with the aim of enhancing the interaction between the three diffusive flows. Experimental investigation of the theoretical predictions has been carried out for infinite and finite couple boundary conditions. The four independent diffusion coefficients in the copper-rich copper-zinc-tin system have been measured at two temperatures for the dilute composition range.

ACKNOWLEDGMENTS

The author is indebted to Dr. J.S. Kirkaldy for suggesting the problem and for his advice and encouragement during the course of this work. Thanks are also due to Drs. G.R. Purdy, L.C. Brown, and J.E. Lane and to Mr. D. Weichert for helpful discussions and assistance throughout this programme.

The author wishes to thank Professor R.E. Ogilvie and his students at M.I.T. for making available the electron probe with which the first results were obtained. The help of Dr. S. Moll at Applied Metals Research Corporation in obtaining the final results is also appreciated.

Acknowledgment is also made of the financial assistance through Annual Grant A697 to Dr. Kirkaldy from the National Research Council of Canada.

TABLE OF CONTENTS

INTRODUCTION

Chemical diffusion is an irreversible atomic mixing of matter in the condensed or gaseous states. In order to discuss diffusion in a quantitative manner the ratio of flow to concentration gradient known as the diffusion coefficient (with dimensions cm^2/sec) has been introduced. In a binary solid state metallurgical system, a simple and straightforward way of evaluating the one independent diffusion coefficient is to weld two pieces of alloy together and to heat this "couple" for sufficient time at high temperature that considerable mixing of material results. From a measure of the concentration profile on both sides of the weld interface, the diffusion coefficient can be evaluated.

In ternary systems there are four independent coefficients which must be determined. These describe not only the flow of each of the two solute elements but also the interaction of these flows.

In this thesis, an investigation of various couple designs is discussed with the aim of enhancing the interaction of the independent atomic flows. The designs discussed include an infinite couple, a semi-infinite couple with reflection from the boundaries, a two phase infinite couple and a steady-state diffusion couple. In addition, the diffusion coefficients in the copper-zinc-tin system are evaluated in the dilute zinc-tin range.

Two methods were used to obtain the concentration profiles in the standard semi-infinite diffusion couples. The x-ray fluorescent

spectrometer was calibrated against standards for the analysis of zinc and tin in copper base alloys with results very similar to Bareham and Fox (1). Although this method of analysis was used only in the preliminary runs it shows excellent possibilities as a quick and accurate quantitative tool. By the proper choice of intensity peak, the depth of x-ray penetration can be reduced to a few microns and the result can be assumed to be a surface analysis. The disadvantage of a large specimen size (one inch in diameter) and the problem of sectioning were completely overcome by the use of the electron probe micro-analyser (2). The micro-analyser can measure the concentrations of three elements simultaneously in a spot two microns in diameter.

The accuracy obtained by either of these methods is better than most analytical techniques and is comparable to tracer or activation analysis (11) except at very low concentrations.

THEORETICAL CONSIDERATIONS

a) Phenomenological Theory of Diffusion

Adolf Fick (3) stated the phenomenological basis of diffusion analysis. He proposed a linear relationship between the diffusive flow, J, and the concentration gradient ∇C, of the form

$$J = - D \nabla C \qquad (1)$$

where the proportionality constant D is called the diffusion coefficient. This has come to be known as Fick's First Law. Since D is often found to be a function of the concentration, Equation (1) is really to be regarded as a definition of the diffusion coefficient.

By combining Equation (1) with the mass balance

$$\text{div } J = - \frac{\partial C}{\partial t} \qquad (2)$$

one obtains the time dependent equation known as Fick's Second Law,

$$\frac{\partial C}{\partial t} = \nabla \cdot \left[D(C) \nabla C \right] \qquad (3)$$

Equations (1) and (3) are sufficient to describe binary volume diffusion in crystals whatever the mechanism of diffusion.

Boltzmann (4) demonstrated how to reduce the partial differential Equation (3) to an ordinary differential equation by introducing the single variable $\lambda = \frac{x}{\sqrt{t}}$. On substitution, Equation (3) becomes

$$- \frac{1}{2} \lambda \frac{dC}{d\lambda} = \frac{d}{d\lambda} \left(D \frac{dC}{d\lambda} \right) \qquad (4)$$

Provided the boundary and initial conditions on C can also be expressed in terms of λ , C will be a solution of this equation. The semi-infinite diffusion couple has this property.

Multiplying throughout by $d\lambda$ and transposing gives

$$d\left(D\frac{dC}{d\lambda}\right) = -\frac{1}{2}\lambda\, dC \tag{5}$$

Integrating from the boundary value $C = C'$ (Where $\frac{dC}{d\lambda} = 0$) to C gives

$$D\frac{dC}{d\lambda}\bigg|_{C} = -\frac{1}{2}\int_{C'}^{C}\lambda\, dC \tag{6}$$

or

$$D(C) \quad \frac{-\frac{1}{2}\int_{C'}^{C}\lambda\, dC}{\frac{dC}{d\lambda}\Big|_{C}} \tag{7}$$

This so-called Boltzmann-Matano Analysis (7) is used to evaluate D from experimental diffusion penetration curves as demonstrated in Figure (1). It should be noted that the so-called Matano interface, the origin of the distance axis as shown in Figure 1 must be chosen so that the two shaded areas are equal. This takes into account the movement of the original weld interface due to the Kirkendall Effect (8).

Binary Diffusion With Constant Coefficients

For the special case where the diffusion coefficient is constant, equation (4) can be written for flow in the x direction

$$-\frac{\lambda}{2D}\frac{dC}{d\lambda} = \frac{d^2C}{d\lambda^2} \tag{4a}$$

Letting $\frac{dC}{d\lambda} = y$ and $\frac{d^2C}{d\lambda^2} = \frac{dy}{d\lambda}$, equation (4a) can be written

$$-\frac{\lambda}{2D} = \frac{d}{d\lambda} \ln y \tag{8}$$

or

$$-\frac{\lambda}{2D} d\lambda = d \ln y \tag{8a}$$

Integration gives

$$\ln y = -\frac{1}{2D}\int \lambda \, d\lambda + \ln A \tag{9}$$

where A is a constant of integration or

$$\frac{dC}{d\lambda} = y = A \exp\left(-\frac{1}{2D}\int \lambda \, d\lambda\right) \tag{9a}$$

Integrating a second time results in

$$C = B + A\int \exp\left(-\frac{\lambda^2}{4D}\right) d\lambda \tag{10}$$

where B is the second constant of integration. For the boundary conditions of an infinite couple

$$C = C' \text{ at } \lambda = -\infty$$
$$C \quad C^{o} \text{ at } \lambda = +\infty \tag{11}$$

Equation (10) becomes

$$C = C^{o} + (C' - C^{o}) \frac{\int_{\lambda}^{\infty} e^{-\frac{\lambda^2}{4D}} \, d\lambda}{\int_{-\infty}^{+\infty} e^{-\frac{\lambda^2}{4D}} \, d\lambda} \tag{10a}$$

where the denominator is the normalizing factor. The solution of the diffusion equation for constant D thus becomes,

$$C = C^{o} + \tfrac{1}{2}\left(C' - C^{o} \right)\left(1 - \frac{2}{\sqrt{\pi}} \int_{0}^{\frac{\lambda}{2\sqrt{D}}} e^{-\xi^2} \, d\xi \right) \tag{11a}$$

or

$$C = C^{o} + \tfrac{1}{2}\left(C' - C^{o} \right)\left(1 - \operatorname{erf} \frac{\lambda}{2\sqrt{D}} \right) \tag{11b}$$

where values of the error function can be obtained from a standard table (6) of functions.

b) Generalized Phenomenological Equations

Onsager (9) proposed, as a generalization of Fick's First Law to multicomponent systems, that the flux of each component be assumed a linear function of all concentration gradients.

$$J_i = - \sum_{k=1}^{n} D'_{ik} \nabla C_k \quad (i = 1, 2, \ldots n) \tag{12}$$

By combining Equations (12) with the mass balances

$$\text{div } J_i + \frac{\partial C_i}{\partial t} = 0 \quad (i = 1, 2, \ldots n) \tag{13}$$

one obtains the generalized diffusion equations

$$\frac{\partial Ci}{\partial t} = \sum_{k=1}^{n} \nabla \cdot (D'_{ik} \nabla C_k) \quad (i = 1, 2, \ldots n) \tag{14}$$

Thus in general, n^2 coefficients D_{ik} which are usually all functions of concentration are required to completely describe the system. However, if the concentration units are chosen such that

$$\sum_{i=1}^{n} C_i = \text{constant} \tag{15}$$

equation (12) can be written

$$J_i = -\sum_{i\ 1}^{n-1} D_{ik} \nabla C_k \qquad (i = 1, 2, \ldots . n - 1) \qquad (12a)$$

where

$$D_{ik} = D'_{ik} - D'_{in} \qquad (16)$$

Thus the number of coefficients to be determined is reduced to $(n - 1)^2$ and equation (14) can be written

$$\frac{\partial C_i}{\partial t} = \sum_{k=1}^{n-1} \nabla.(D_{ik} \nabla C_k) \qquad (i = 1, 2, \ldots . n - 1) \qquad (17)$$

Kirkaldy (10) has stated the ternary analogue to the Boltzmann-Matano analysis. For diffusion in the x direction, parametric solutions of the form

$$C_i = C_i(\lambda), \qquad \lambda = \frac{x}{\sqrt{t}} \qquad (18)$$

are sought for Equation (17). The resulting set of non-linear ordinary differential equations is

$$-\frac{\lambda}{2} \frac{dC_i}{d\lambda} = \sum_{k=1}^{n-1} \frac{d}{d\lambda} \left[D_{ik} \frac{dC_k}{d\lambda} \right] \qquad (19)$$

The first integration of Equation (19) with semi-infinite boundary conditions

$$C_i = C_i^o \quad \text{for } x>0 \text{ and } t = 0 \quad (\text{ie. } \lambda = +\infty)$$
$$C_i = C_i' \quad \text{for } x<0 \text{ and } t = 0 \quad (\text{ie. } \lambda = -\infty) \tag{20}$$

gives

$$\frac{1}{2}\int_{C_i^o}^{C_i} \lambda \, dC_i = \sum_{k=1}^{n-1} D_{ik} \left.\frac{dC_k}{d\lambda}\right|_{C_k} \tag{21}$$

Since the integral can be evaluated graphically and the slopes $\frac{dC_k}{d\lambda}$ can be measured from experimental curves, Equation (21) can be used for determining concentration dependent coefficients. Mason (11) has outlined the procedure to be used to determine concentration - dependent diffusion coefficients for a three component system.

Ternary Diffusion With Constant Coefficients

Gosting & Fujita (5) and Kirkaldy (14) have shown that in the special case where the D's are constant and where n = 3, the solutions of Equation (19) can be written

$$C_1 = a \operatorname{erf} \frac{\lambda}{2\sqrt{u}} + b \operatorname{erf} \frac{\lambda}{2\sqrt{v}} + c \tag{22}$$

and

$$C_2 = d \operatorname{erf} \frac{\lambda}{2\sqrt{u}} + e \operatorname{erf} \frac{\lambda}{2\sqrt{v}} + f \tag{23}$$

where

$$a = \frac{1}{2D}\left\{D_{12}\,(C_{20}-C_{21}) - \left[(D_{22}-D_{11})-D\right]\left(\frac{C_{10}-C_{11}}{2}\right)\right\}$$

$$b = \frac{1}{2}\left\{C_{10} - C_{11} - 2a\right\}$$

$$c = \frac{1}{2}\left\{C_{10} + C_{11}\right\}$$

$$d = \frac{1}{2D}\left\{D_{21}\,(C_{10}-C_{11}) - \left[(D_{11}-D_{22})-D\right]\left(\frac{C_{20}-C_{21}}{2}\right)\right\}$$

$$e = \frac{1}{2}\left\{C_{20} - C_{21} - 2d\right\}$$

$$f = \frac{1}{2}\left\{C_{20} + C_{21}\right\}$$

$$u = D_{11} + \frac{1}{2}\left\{(D_{22} - D_{11}) + D\right\}$$

$$v = D_{22} + \frac{1}{2}\left\{(D_{11} - D_{22}) - D\right\}$$

$$D = \sqrt{(D_{11} - D_{22}) + 4D_{12}D_{21}}$$

Solutions (22) and (23) are for infinite couples subject to the initial conditions

$$C_i = C_{io} \quad \text{for } x > 0 \quad \text{and} \quad t = 0$$

$$C_i = C_{i1} \quad \text{for } x < 0 \quad \text{and} \quad t = 0 \qquad (24)$$

c) Thermodynamic Interpretation of the Phenomenological Diffusion Equations

Kirkaldy et al (13) have considered ternary diffusion in substitutional systems where the two substitutional components (1 and 2) are diffusing in a matrix of the third element (3). In this case, Equation (12a) can be written for the flow of component one in the x direction

$$J_1 = - D_{11} \frac{\partial C_1}{\partial x} - D_{12} \frac{\partial C_2}{\partial x} \qquad (12b)$$

An alternative expression written in terms of potential gradients is

$$J_1 = - L_{11} X_1 - L_{12} X_2 \qquad (25)$$

where the X's are independent forces. In a number fixed frame of reference,

$$X_1 = \left(1 + \frac{C_1}{C_3} \right) \frac{\partial \mu_1}{\partial x} + \frac{C_2}{C_3} \frac{\partial \mu_2}{\partial x} \qquad (26)$$

where the concentrations C, are measured in atom percent and the plane of reference corresponds to the Matano interface (for which the number of atom sites remains constant on both sides).

If one introduces into (25) and (26)

$$\mu_1 = \mu_1 (C_1 , C_2) \tag{27}$$

then by comparison with (12b), one obtains the ratio,

$$\frac{D_{12}}{D_{11}} = \frac{\left\{ \left(1 + \frac{C_1}{C_3} \right) \frac{\partial \mu_1}{\partial C_2} + \frac{C_2}{C_3} \frac{\partial \mu_2}{\partial C_2} \right\} L_{11}}{\left\{ \left(1 + \frac{C_1}{C_3} \right) \frac{\partial \mu_1}{\partial C_1} + \frac{C_2}{C_3} \frac{\partial \mu_2}{\partial C_1} \right\} L_{11}}$$

$$+ \left\{ \left(1 + \frac{C_2}{C_3} \right) \frac{\partial \mu_2}{\partial C_2} + \frac{C_1}{C_3} \frac{\partial \mu_1}{\partial C_2} \right\} L_{12}$$

$$+ \left\{ \left(1 + \frac{C_2}{C_3} \right) \frac{\partial \mu_2}{\partial C_1} + \frac{C_1}{C_3} \frac{\partial \mu_1}{\partial C_1} \right\} L_{12} \tag{28}$$

Subject to the approximation that the off-diagonal interactions L_{12} are small, Equation (28) reduces to

$$\frac{D_{12}}{D_{11}} = \frac{\left(1 + \frac{C_1}{C_3} \right) \frac{\partial \mu_1}{\partial C_2} + \frac{C_2}{C_3} \frac{\partial \mu_2}{\partial C_2}}{\left(1 + \frac{C_1}{C_3} \right) \frac{\partial \mu_1}{\partial C_1} + \frac{C_2}{C_3} \frac{\partial \mu_2}{\partial C_1}} \tag{29}$$

The corresponding relation for component two can be obtained by an exchange of subscripts.

By means of a statistical calculation based on nearest

neighbour interactions, these authors have expanded the chemical potentials as

$$\mu_1 = \mu_1^\circ + RT\,(\ln C_1 + \varepsilon_{11}C_1 + \varepsilon_{12}C_2) \tag{30}$$

$$\mu_2 = \mu_2^\circ + RT\,(\ln C_2 + \varepsilon_{22}C_2 + \varepsilon_{21}C_1) \tag{31}$$

where the μ°'s are standard chemical potentials, the ε's are sums of pair interaction energies divided by kT and the C's are concentrations expressed in atom fractions. A Maxwell thermodynamic relation applied to the above leads to the symmetry relation $\varepsilon_{12} = \varepsilon_{21}$.

Substituting (30) and (31) into (28) and its symmetrical counterpart gives

$$\frac{D_{12}}{D_{11}} = \frac{C_1 + C_1C_3\varepsilon_{12}}{1 - C_2 + C_1C_3\varepsilon_{11}} \tag{32}$$

$$\frac{D_{21}}{D_{22}} = \frac{C_2 + C_2C_3\varepsilon_{12}}{1 - C_1 + C_2C_3\varepsilon_{22}} \tag{33}$$

For dilute solutions in which C_1 and $C_2 << 1$, (32) and (33) reduce to

$$\frac{D_{12}}{D_{11}} = (1 + \varepsilon_{12})\,C_1 \tag{34}$$

$$\frac{D_{21}}{D_{22}} = (1 + \varepsilon_{12}) C_2 \qquad (35)$$

These equations are applicable only to dilute solutions, and even then their validity depends upon the neglect of the Onsager interaction terms, L_{12} and L_{21}. Statistical theory indicates that the latter is probably not very good for substitutional solution.

d) Couple Designs for Enhanced Off-Diagonal Effect

In order to compare the above theoretical predictions with experimental results, it is necessary to design the experiment so that the off-diagonal coefficients are easily measurable. Past experience has taught us that the cross-effects are significant only when at least one of the independant concentration differences is as large as possible (15) and it has also become apparent that there is a strong tendency for the cross-effects to become moderated when the two on-diagonal coefficients D_{11} and D_{22} are of the same order of magnitude (16). A number of possible couple designs are discussed below with reference to these difficulties.

1) Steady-State Diffusion

Although most diffusion studies have been made under unsteady-state conditions, it is known (17) that the steady state method is often superior with respect to the directness and accuracy of interpretation of the data. This is certainly true where one of the solute components (component 2) has a high vapour pressure so that the chemical potential of this component can be controlled on both sides of a thin membrane of solvent material containing small amounts of the other component (component 1) in solid solution.

When the steady-state is reached, the flux of component two, J_2, will be some finite constant value while the flux of component 1 will be zero. Thus from equation (12a) one can write for diffusion in the x direction

$$- J_1 = 0 = D_{11} \frac{dC_1}{dx} + D_{12} \frac{dC_2}{dx} \tag{36}$$

or

$$D_{11}\, dC_1 + D_{12}\, dC_2 = 0 \tag{37}$$

Assuming the D's constant and integrating between the limits shown gives

$$D_{11} \int_{C_{11}}^{C_{10}} dC_1 + D_{12} \int_{C_{21}}^{C_{20}} dC_2 = 0 \tag{38}$$

or

$$C_{11} - C_{10} = \frac{D_{12}}{D_{11}} (C_{20} - C_{21}) \tag{39}$$

Equation (39) can be written

$$\Delta C_1 = \frac{D_{12}}{D_{11}} \frac{C_{20} - C_{21}}{2} \tag{40}$$

where ΔC_1 is the difference between the maximum concentration induced by the cross-effect and the mean concentration of component one.

Equation (40) shows the very simple linear relationship between ΔC_1, the quantity to be measured and $C_{20} - C_{21}$, the concentration gradient of component two across the membrane which can be controlled by the

experimenter. The proportionality constant in Equation (40), D_{12}/D_{11}, can thus be determined and the off-diagonal diffusion coefficient D_{12} can be evaluated.

The ease of analysis of the steady state makes this type of experiment very attractive if the diffusion time required is not prohibitive. Kirkaldy and Purdy (18) have used a special case of the steady state in their "transient equilibrium" interstitial diffusion studies.

ii) The Infinite Couple

Amplification of the off-diagonal effect with an infinite couple is usually achieved by setting the composition of one component (C_1) constant throughout at t = 0 and by having a step distribution in component two (11,15). Redistribution of component one will be caused primarily by the off-diagonal coefficient D_{12} while the distribution of component two will not be altered appreciably by the small concentration gradient induced in component one. Thus in this situation, $D_{21} \frac{d^2C_2}{d\lambda^2}$ can be set equal to zero, which is equilvalent to setting $D_{21} = 0$ in relations (22) and (23).

Kirkaldy et al (13) have calculated the maximum change (ΔC_1) in C_1 from its uniform composition with infinite couple boundary conditions for various D_{22}/D_{11} ratios, since the magnitude of ΔC_1 is an index of the measurability of the coefficient D_{12}. Their result, coming from Equation (22) is

$$\Delta C_1 = k(\phi) \frac{D_{12}}{D_{11}} \left(\frac{C_{20} - C_{21}}{2} \right) \qquad (41)$$

These authors show that $k(\phi)$ varies between unity for $\phi \ll 1$ and zero for $\phi \gg 1$ as a monotonic function of ϕ as shown in Figure 2.

For the special case of $D_{11} = D_{22}$ which is a quite likely situation in substitutional diffusion, the result can be obtained from Equation (22) as

$$C_1 = \frac{1}{\sqrt{2\pi e}} \frac{D_{12}}{D_{11}} \frac{C_{20} - C_{21}}{2} \tag{42}$$

or

$$C_1 = 0.242 \frac{D_{12}}{D_{11}} \frac{C_{20} - C_{21}}{2} \tag{43}$$

This expression shows very vividly the moderating effect in relation to the steady state result and the consequent difficulty of measuring D_{12} due to the on-diagonal coefficients D_{11} and D_{22} being of the same order of magnitude.

iii) Reflection from a Boundary

In the infinite couple discussed above, ΔC_1 is small because component one diffuses rapidly in a direction to remove the perturbation caused by the diffusion of component two. As a result, the position of the maximum ΔC_1 is well removed from the Matano interface.

It appeared possible to increase the magnitude of ΔC_1 by introducing into the system a reflecting boundary at which component one would be stopped and forced to pile up. Weichert (12) has given an approximate solution to this problem using the model of a finite couple with reflection at the boundaries shown in Figure 3. Initially

$$C_2 = C_{20} \quad \text{at} \quad -\xi < x < \xi$$

$$C_2 = C_{21} \quad \text{at} \quad -L < x < -\xi \quad \text{and} \quad \xi < x < L \tag{44}$$

$$\text{and } C_1 = C_{10} \quad \text{at} \quad -L < x < L$$

The result, in matrix notation for constant coefficients is to a good approximation,

$$\Delta C_k = \sum_{m=1}^{\infty} \frac{2(C_{20} - C_{21})(-1)^{m+1}}{(D_{22} - D_{11})\pi(2m-1)}$$

$$\begin{pmatrix} D_{12} & -D_{12} \\ D_{22} - D_{11} & D_{11} - D_{22} \end{pmatrix} \begin{pmatrix} e^{-D_{22}\lambda_m^2 t} \\ e^{-D_{11}\lambda_m^2 t} \end{pmatrix} \cos \lambda_m t \tag{45}$$

where $\lambda_m = (2m-1)\frac{\pi}{L}$, subject to the condition that $D_{11} \approx D_{22}$. At long times, Equation (45) can be approximated by a single cosine term corresponding to $m = 1$ since the higher harmonics, $m = 3, 5, \ldots$, have reached their maxima and decayed. Thus,

$$\Delta C_1 \quad \frac{2}{\pi} \frac{(C_{20}-C_{21})D_{12}}{(D_{22}-D_{11})} \left[e^{-D_{22}\lambda_m^2 t} - e^{-D_{11}\lambda_m^2 t} \right] \cos \lambda_m t \tag{45a}$$

Maximixing ΔC_1 with respect to time and substituting the value of the optimum time into Equation 45a, one obtains the expression

$$\Delta C_1 = k(\alpha) \frac{D_{12}}{D_{11}} \left(\frac{C_{20} - C_{21}}{2} \right) \qquad (45b)$$

where $\alpha = \frac{D_{22}}{D_{11}}$ and $k(\alpha) = \frac{4}{\pi(\alpha - 1)} \left[e^{-\frac{\alpha \ln \alpha}{\alpha - 1} - \frac{\ln \alpha}{\alpha - 1}} \right]$

However, when $\alpha > 1$, the time necessary for component one to attain its maximum concentration difference, ΔC_1, cannot be reached before the concentration step in component two is moderated. In this case, higher harmonics will produce perturbations at the points $\pm \frac{n}{5}$. The curve of $k(\alpha)$ versus α over the range $0.4 < \alpha < 1$ (where $D_{11} \approx D_{22}$) is shown in Figure 2. Beyond the point $\alpha = 1$, $k(\alpha)$ as here defined loses its physical significance since the approximations become invalid.

From Figure 2, it is obvious that the finite couple will approximately double the concentration change to be expected in an infinite couple of the same compositions in the range $0.4 < \alpha < 1$. This is a significant gain, but still far short of that to be obtained in a steady-state couple.

iv) Diffusion in a Two Phase System

The necessity of having one of the independent concentration differences as large as possible has been stressed above as a criterion for a measurable off-diagonal effect. If the solubility limits of the solute species in the solvent are high enough to produce the required concentration differences, one of the couple designs mentioned above can be used to determine off-diagonal diffusion coefficients. However, if one

species has a restricted solubility limit, as for example the low solubility of manganese in aluminum in the investigation of Mason (11), a possible method of increasing the concentration differences is through use of a two phase diffusion couple.

As an example, let us consider the copper-rich corner of the Cu-Zn-Sn isotherm at 500°C (Figure 4). It appears possible to increase the effective concentration differences across a couple by using a composition A rather than B (where A and B are the ends of a tie line) for one half of a diffusion couple. It would thus appear that couples of the form A-C and A-D would give enhanced concentration differences across the interface compared to the single phase couples BC and BD in the component which was initially uniform. To determine the enhancement to be expected, it is sufficient to estimate the composition profile of component two (which contained the concentration step). It can be seen that the solution

$$C(\lambda) = C_{21} \frac{\operatorname{erfc}\left(-\frac{\lambda}{2\sqrt{D}}\right)}{\operatorname{erfc}\left(-\frac{\alpha}{2\sqrt{D}}\right)} \tag{46}$$

fits the boundary conditions

$$\begin{aligned} C &= C_{21} \quad \text{at} \quad \lambda = \alpha \\ C &= 0 \quad \text{at} \quad \lambda = -\infty \end{aligned} \tag{47}$$

The value of α must be determined through the mass balance at the interface as seen in Figure 5.

$$\alpha C_{22} - \int_0^{\infty} C_{21} \frac{\operatorname{erfc}\left(-\frac{\lambda}{2\sqrt{D}}\right)}{\operatorname{erfc}\left(-\frac{\alpha}{2\sqrt{D}}\right)} d\lambda = \int_{-\infty}^{0} C_{21} \frac{\operatorname{erfc}\left(-\frac{\lambda}{2\sqrt{D}}\right)}{\operatorname{erfc}\left(-\frac{\alpha}{2\sqrt{D}}\right)} d\lambda \qquad (48)$$

or

$$\alpha C_{22} = 2\sqrt{D} \int_0^{\beta} C_{21} \frac{\operatorname{erfc}(-y)}{\operatorname{erfc}(-\beta)} dy + 2\sqrt{D} \int_{-\infty}^{0} C_{21} \frac{\operatorname{erfc}(-y)}{\operatorname{erfc}(-\beta)} dy \qquad (49)$$

where $y = \frac{\lambda}{2\sqrt{D}}$ and $\beta = \frac{\alpha}{2\sqrt{D}}$

Thus (49) can be written

$$\beta C_{22} = \frac{C_{21}}{\operatorname{erfc}(-\beta)} \left[\int_0^{\beta} \operatorname{erfc}(-y)dy + \int_{-\infty}^{0} \operatorname{erfc}(-y)dy \right] \qquad (50)$$

$$\left[\int_0^{\beta} \left\{2-\operatorname{erfc}(y)\right\} dy - \int_{\infty}^{0} \operatorname{erfc}(y)dy \right] \qquad (51)$$

$$\left[2\beta - \int_0^{\infty} \operatorname{erfc}(y)dy + \int_{\beta}^{\infty} \operatorname{erfc}(y)dy + \int_0^{\infty} \operatorname{erfc}(y)dy \right] \qquad (52)$$

Thus the equation becomes

$$\beta C_{22} = \frac{C_{21}}{\operatorname{erfc}(-\beta)} \left[2\beta - \operatorname{ierfc}(0) + \operatorname{ierfc}(\beta) + \operatorname{ierfc}(0) \right] \qquad (53)$$

since

$$\int_{x}^{\infty} \operatorname{erfc}(z)dz \equiv \operatorname{ierfc}(x)$$

Therefore

$$\frac{C_{22}}{C_{21}} = \frac{2}{\operatorname{erfc}(-\beta)} + \frac{\operatorname{ierfc}(\beta)}{\beta(\operatorname{erfc}(-\beta)} \tag{54}$$

Taking component two to be tin, the concentrations expressed in atom fractions are $C_{22} = 0.208$ and $C_{21} = 0.0733$. Using these values of concentration, a value of $\beta = 0.22$ was iterated from the graphical representation given by Weichert (12) for the various β functions in Equation (54).

Substituting $\beta = 0.22$ into Equation (46) gives

$$C(\lambda) = \frac{C_{21}}{1.24} \left(2 - \operatorname{erfc} \frac{\lambda}{2\sqrt{D}} \right) \tag{55}$$

This can be compared to the solution for an infinite couple with an initial concentration step of C_{21} at the origin

$$C(\lambda) = \frac{C_{21}}{2} \left[\operatorname{erfc} \left(- \frac{\lambda}{2\sqrt{D}} \right) \right] \tag{56}$$

or

$$C(\lambda) = \frac{C_{21}}{2} \left[2 - \operatorname{erfc} \left(\frac{\lambda}{2\sqrt{D}} \right) \right] \tag{57}$$

Equation (57) satisfies the boundary conditions that

$$C(\lambda) = \frac{C_{21}}{2} \quad \text{at} \quad \lambda = 0$$

$$C(\lambda) = C_{21} \quad \text{at} \quad \lambda = \infty \tag{58}$$

$$C(\lambda) = 0 \quad \text{at} \quad \lambda = -\infty$$

Comparing (55) and (57), it can be seen that the enhancement obtained in this two phase couple will be approximately 40%. This result can be appreciated when it is remembered that the concentration profile of Equation (55) will remain symmetric about the point $\lambda = 0$.

Equation (46) can be rewritten

$$C(\lambda) = \frac{C_{21}}{2-\operatorname{erfc}(\beta)} \left[2 - \operatorname{erfc}\left(\frac{\lambda}{2\sqrt{D}}\right) \right] \tag{46a}$$

Since the function $\operatorname{erfc}(\beta)$ can take values from 0 to 1, it is a general result that a two phase diffusion couple of the type above can give a maximum enhancement of 100 percent compared to the infinite couple.

FLUORESCENT SPECTROMETRY AND ELECTRON PROBE MICRO-ANALYSIS

The chemical wet procedures, formerly used almost exclusively for the solution of many analyzing problems, are now frequently supplemented or replaced by physical methods. In metallurgical systems, the speed and non-destructive nature of the latter types of quantitative analysis render them invaluable. In particular, x-ray fluorescent spectrometry, and more recently electron probe micro-analysis, have gained increasing importance.

Basically, both techniques rely upon the excitation and detection of the characteristic x-ray spectra of the elements of interest in the alloy to be analyzed. Because of the complex nature of the phenomena of mass absorption and mutual excitation of x-rays in crystalline alloys, no satisfactory method is yet available for the conversion of radiation intensity directly to composition. For this reason, accurate quantitative analysis are obtained by a comparison of the x-ray intensities of standard alloys of known composition and the alloy to be analyzed.

a) Excitation of X-rays in the Electron Probe Micro-analyzer

The electron probe micro-analyzer is basically a primary x-ray tube in which the alloy to be analyzed acts as the target for the high energy electrons emitted from the electron gun. X-rays are produced by either of two processes. The high energy electrons which excite electrons in the target elements into higher energy states generate the characteristic line spectrum of those elements while the electrons that are decelerated in the target produce the continuous or "white" radiation. The resultant spectrum for a pure target is shown schematically in Figure 6 with the K_{α} and K_{β} characteristic peaks.

The continuous spectrum in Figure 6 is characterized by a certain lower cut-off limit, λ_{min} which depends only on the operating voltage, V, according to the Duane-Hunt Law (19).

$$\lambda_{min} = \frac{12,350}{V} \tag{59}$$

This minimum wavelength is independent of the target element. The overall intensity of the spectrum, however, does depend on the atomic number (Z) of the target. This intensity, I_{ν}, as a function of frequency rather than wavelength is given by the relationship

$$I_{\nu} = AZ\,(\nu_0 - \nu) + BZ \tag{60}$$

where A and B are constants and ν_0 is the maximum frequency correspon-

ding to λ_{min}. From Equation (60), it is apparent that a heavy element target will yield more primary x-rays of each wavelength than will a target element of low atomic number.

The characteristic radiation is produced only when the high voltage electrons have sufficient energy to excite an electron in the target element to a higher energy level. This energy varies with the atomic number of the element and is called the K absorption energy or the L absorption energy for the excitation of a K or L electron. Usually, for convenience, the absorption energy is expressed in terms of wavelength as $\lambda_{K_{abs}}$ or $\lambda_{L_{abs}}$.

The extreme usefulness of the electron probe micro-analyzer is due mainly to the fact that the electron beam can be focussed at a spot about two microns in diameter on the surface of the target by means of magnetic lenses and that the target can be moved relative to the point of electron impingement. Under these circumstances, the whole surface area of the target can be analyzed with excellent resolution.

Unfortunately, the high continuous radiation background associated with the spectrum of Figure 6 prevents the detection and analysis of small alloy concentrations. This difficulty is partially overcome in the fluorescent spectrometer.

b) Excitation of X-rays in the Fluorescent Spectrometer

The fluorescent x-ray spectrum is produced when x-rays of sufficient energy from a primary x-ray source impinge upon a specimen. The voltage in the primary tube necessary to excite the fluorescent spectrum, V_f, is given by the relation

$$V_f = \frac{12,350}{\lambda_{K_{abs}}} \qquad (59a)$$

The intensity of fluorescent yield increases rapidly with operating voltage and target element atomic number in the primary x-ray tube. Consequently, the primary tube is operated with a tungsten or molybdenum target at a voltage well above that required by Equation (59a).

The characteristic spectral lines of both the primary and fluorescent spectra can be illustrated as transitions on an electron energy level diagram shown schematically in Figure 7 for a heavy atom. If a primary x-ray quantum, whether from the continuous or characteristic spectrum, removes a "K" electron, the vacancy can be filled by an electron from the L or M shell, with the emission of a quantum of electromagnetic radiation characteristic of the energy level change. The relation between the energy change, E, and the wavelength of the x-ray quantum, λ, is given by the well known relation

$$E = h/\lambda \qquad (61)$$

where h is Planck's constant. The system of nomenclature is obvious

from Figure 7.

The continuous or "white" radiation of the primary spectrum has no counterpart in the fluorescent spectrum since x-rays cannot lose their energy in a continuous manner analogous to the deceleration of electrons. Part of the background in fluorescent spectra is the result of primary radiation scattered from the sample, while the remainder is caused mainly by scattering of the fluorescent yield in the analyzing crystal. The latter can be eliminated in the detection electronics by proper pulse amplitude discrimination while the former, being of the same wavelength as that part of the spectrum on which it is superimposed, cannot be supressed. This background radiation is the result of coherent and Compton scattering of x-rays.

Coherent scattering results from the elastic interaction between an x-ray quantum and a tightly bound electron. Since the recoil of the electron and nucleus is negligible, the quantum recoils with no loss in energy and the scattered radiation is of the same wavelength as the primary radiation.

Compton scattering or modified radiation is the result of an encounter of a quantum with a loosely bound or a free electron in which the electron recoils under the impact and the quantum is deflected with a partial loss of energy. Since the laws of conservation of energy and momentum apply, an expression can be derived relating the angle of scatter (ϕ) to the loss of energy in the encounter and thus the increase in wavelength ($\Delta\lambda$) of the quantum.

$$\Delta\lambda = \frac{h}{mc} \left(1 - \cos\phi \right)$$

or (62)

$$\Delta\lambda = 0.024 \left(1 - \cos\phi \right)$$

where h is Planck's constant, m is the mass of the electron and C is the velocity of light. In the heavier elements, more of the electrons are tightly bound and contribute to coherent rather than Compton scattering.

c) Analysis of the Spectra

Once the characteristic x-ray spectrum has been excited, it is necessary to distinguish the various wavelengths. Because of the high resolution afforded by dispersive x-ray optics, diffraction of x-rays from analyzing crystals is usually chosen as the basis for spectral analysis. Figure 8 shows a simplified schematic representation of the x-ray path in a flat crystal dispersive system.

The wave lengths of the emitted x-ray quanta are determined with the aid of the x-ray diffraction produced by the atoms of the analyzing crystal lattice. The diffraction angles are found by means of Bragg's "reflection formula", viz.

$$n\lambda = 2d \sin\theta \qquad n = 1, 2, 3, \ldots\ldots \tag{63}$$

Accordingly, a lattice-plane family of a crystal lattice with the interplane distance d can only "reflect" x-rays of the wavelength λ if the angle of incidence θ of the beam of rays conforms to this equation, in which n denotes the order of reflection. The angle between the incident beam and the reflecting family of planes of the analyzer crystal is equal to that between the family of planes and the diffracted beam. The incident and the reflected beams form together an angle of 2θ as seen in Figure 8. The measurement of 2θ enables a clear inference to be drawn as to the wave lengths of the emitted spectra.

The choice of analyzer crystal is dictated by the dispersion relation

$$\frac{d\theta}{d\lambda} = \frac{n}{2d \cos\theta} \qquad (64)$$

The dispersion of the spectrum is inversely proportional to the lattice constant d. For this reason, analyzer crystals are chosen which have as small a lattice constant as possible besides satisfactory reflecting and radiation resisting properties. Lithium fluoride with d = 2.01 A^{o} is chiefly used.

It is apparent from Figure 8 that for continuous scanning through the various wavelengths, the analyzer crystal and the detector must be coupled so that the former rotates through an angle θ while the latter rotates through 2θ . This configuration is achieved in the diffractometer with the analyzer crystal at the goniometer axis and the detector rotating about this axis at twice the angular velocity of the crystal. The proper 2θ setting of the detector for the various spectral lines of the elements can be found in standard conversion tables (20) for a number of common analyzer crystals. These conversion tables also make possible the reverse process; the identification of unknown species in the sample under analysis.

i) The Scintillation Counter

The x-ray detector used in conjunction with the diffractometer should have the characteristics of a high counting rate ($\sim 10^{6}$ quanta/sec) and a proportionality between quantum energy imput and signal energy output. Both of these features are found in the scintillation counter.

The scintillation counter consists of a luminescent material such as a thallium activated sodium-iodide crystal block and a photomultiplier.

X-ray quanta absorption in the crystal block causes pulses of visible light to be emitted by the crystal atoms which are detected and amplified by the photomultiplier. The number of light pulses generated depends on the energy of the x-ray quantum so when the scintillation counter is used in conjunction with a pulse height analyzer, a narrow energy or wave-length range of the spectrum can be sorted out. Thus only x-ray quanta within this energy band will be recorded and all other pulses will be rejected by the electronic circuitry.

Another distinct advantage of the scintillation counter is its high stability. The high voltage versus intensity characteristics illustrated schematically in Figure 9 show a long flat plateau. At a lower value of the H.T., the pulse-amplification is not yet sufficient for all the pulses to pass the sensitivity threshold of the counting electronics. At higher values of the H.T., the noise amplitudes of the multiplier tube are amplified so much that these too are counted, resulting in a high background. By choosing a H.T. value at the lower side of the plateau, voltage fluctuations in the high voltage to the scintillation counter have almost no effect on the overall intensity output, thus leading to a highly stable mode of operation.

ii) Instrumentation

The counting instrumentation to be discussed below was supplied by Philip's Industries Limited for use with their commercial x-ray fluorescent spectrometer unit, PW 1540. Although many commercial electron-probe microanalyzers do not use these exact components, they serve as a basic counting unit which could be applied to the analysis of any x-ray spectrum. In particular, this basic unit will be incorporated in the

electron probe micro-analyzer designed by Dr. G.R. Purdy, which is now under construction at McMaster University.

The components are:

1. PW 1964/10, a scintillation counter consisting of a thalluim activated NaI crystal for detecting the radiation, a photomultiplier tube with eleven dynodes, and a cathode follower.
2. PW 4024, a stabilized high voltage power supply which can supply the scintillation probe, PW 1964/10, to a maximum of 2500 volts. In cases of fluctuations in the mains of 10%, the deviation of the high voltage output is less than 0.05%.
3. PW 4072/01, a linear amplifier which amplifies pulses of varying amplitude. The unit amplifies pulses with a gain of 2400 and input attenuation facility of 1x, 2x, 4x, 8x, 16x, 32x, and 64x.
4. PW 4029/01, a stabilized power supply designed to supply, PW 4024, with power. The deviation is less than 0.1% of the mains fluctuation.
5. PW 4082, a single channel pulse height analyzer to separate pulses with different amplitudes and thereby to analyze the energy spectrum of radiation. On threshold discrimination settings all pulses above the adjusted voltage are counted. Using channel discrimination all pulses within a set "window" of voltages are recorded. The channel width is adjustable to 1, 2, 4, 8, 12, 16, 20, 24, 28 or 32 volts. The centre of the voltage range within the channel is the channel height and is adjustable to any value between 4 and 100 volts.
6. PW 4032, a universal scalar, used for counting pulses up to a maximum of 4×10^5. Settings for total counts are 1, 2 or 4 times 10, 10^2, 10^3, 10^4, or 10^5.

7. PW 4052, a preset-count unit, used for measuring the time in which a predetermined number of pulses are registered on the universal scalar, PW 4032.

8. PW 4042, a ratemeter, used to check instantaneously the radiation intensity and to determine any variations of intensity with time.

d) Calibration

The most accurate quantitative results can be obtained by a comparison of the x-ray intensities of the sample to be analyzed and standards of known composition. An alternative approach, due to Castaing (21), is the correction of the x-ray intensities for background, absorption effects, fluorescent effects and atomic number differences. The inherent errors of this second method make the first approach more attractive if homogeneous standards can be prepared.

i) Preparation of Standards

The calibration standards for both the x-ray fluorescent spectrometer and the electron probe micro-analyzer were prepared to cover the single phase copper rich corner of the Cu-Zn-Sn phase diagram. Because of the diffusion temperatures to be used and the desire for dilute solutions, the composition range was limited to 5 atomic percent (or 5 wt %) Zn and 7 atomic percent tin (or 12 weight %).

The alloys were melted in a clay and graphite crucible in a gas furnace under a borax flux and chill cast into a cold steel mold. The ingots produced were approximately 1 3/4 inches in diameter but the height was limited to about 1 inch in order to induce undirectional solidification from the bottom to the top of the ingot. To moderate the dendritic segregation, the ingots were annealed for one week in a salt pot at 650°C. After this treatment, the ingots were machined to a diameter of 1.25

inches and a thickness of 1/2 to 3/4 inches to remove the surface concentration differences due to dezincification during annealing and inverse segregation during solidification.

Wet chemical analyses of representative samples were carried out at the Canadian Westinghouse Ltd., Research and Development Laboratory in Hamilton. Table I gives the compositions of the alloys used for comparison standards.

ii) Intensity vs Concentration Curves

Calibration curves of intensity versus concentration were obtained for the three instruments used: the Philips x-ray fluorescent spectrometer, the Applied Research Laboratory (A.R.L.) Probe, and the Advanced Metals Research (A.M.R.) Probe. In most cases, the intensities were plotted as a ratio, I/I_0 where I is the x-ray intensity on a given line of the element of interest in the alloy and I_0 is the x-ray intensity of the pure material measured on the same line. Plotting in this way enables one to use the same calibration curves from day to day under changing conditions since the I/I_0 ratio remains constant.

The calibration curves for zinc and tin on the x-ray fluorescent spectrometer are shown in Figures 10 and 11 respectively. In Figure 11, the intensity ratio is not plotted because the very large I_0 value of tin on the Sn K_{α_1} line is beyond the range of the scintillation counter. However both of these curves show linear characteristics as demonstrated earlier by Bareham and Fox (1).

The A.R.L. Probe features a high take-off angle of 52.5°, measured from the plane of the specimen surface to the position of the analyzer crystal. Under these conditions, one expects the x-ray absorption

correction to be very small since the x-rays excited in the sample have a very short path length when they emerge at 52.5°. The small degree of x-ray absorption should result in near-linear calibration curves as shown for zinc and tin in Figures 12 and 13 respectively. Because of the large numbers of data points to be determined, analytical expressions were fitted to these curves by the method of "least squares" with results as shown.

In contrast to the A.R.L. Probe, the take-off angle in the A.M.R. Probe is quite low at 15.5°. However, from the calibration curves for zinc and tin shown in Figures 14 and 15 respectively, it is obvious that the larger absorption effects have still not introduced non-linearity in the concentration versus intensity characteristics. As with the previous data, analytical expressions have been fitted by the method of "least squares" with results as shown.

With the use of the calibration curves shown in Figures 11 through 15, a quick accurate conversion of x-ray intensities to composition can be made. This has been done in the analysis of diffusion data shown in the next section.

EXPERIMENTAL PROCEDURES AND RESULTS

The object of this investigation was to determine experimentaly the off-diagonal diffusion coefficients, $D_{Sn\ Zn}$ and $D_{Zn\ Sn}$, in the copper rich corner of the copper-zinc-tin system. To this end, three types of experiments were designed to produce a measureable cross-effect. These included the steady-state couple, the infinite couple and the finite couple with reflection from a boundary, each of which will be discussed below.

i) Steady-State Diffusion

In the ternary system, the principle of the steady-state diffusion couples is to set up a steady-state zinc gradient varying from zero on one side of the diffusion membrane to some finite value on the other side. The originally uniform tin will then interact with this zinc gradient to produce a measureable cross-effect.

The steady-state diffusion experiments were carried out in the cell shown in Figure 16 which is a modification of that used by Yue and and Guy (22). The molybdenum bolts which held the diffusion membrane between the two stainless steel cups were tightened to finger tightness and the cell was placed in a horizontal vacuum furnace. In this condition, the interior of the cell could be evacuated to the pressure of the furnace (10^{-5}mmHg) before the welding process began. When the desired pressure was reached, the furnace was raised to the diffusion temperature. Due to the much higher thermal expansion of stainless steel

compared to molybdenum, tremendous pressures were exerted on the copper diffusion membrane which led to excellent welds in the couple. The thick copper "O" - ring was inserted on the "sink" side, ie. the side containing the pure copper turnings, so that the cell could be machined apart easily. Preliminary experiments were carried out using copper - 4.85 atom percent zinc turnings as a zinc source and pure copper turnings as sink with pure copper and copper - 4.13 atom percent tin membranes rolled to a thickness of 0.002 inches. Diffusion times and temperatures necessary to obtain the steady-state were taken from Yue and Guy (22).

Although the steady-state couples produces the largest theoretical off-diagonal effect, many technical difficulties must be overcome. Mechanical break-down of the diffusion membrane can be partially overcome by an extended high temperature anneal. In the cooling process after diffusion, pure zinc condenses in globules on the surface which makes surface analyses with the x-ray fluorescent spectrometer impossible although the electron probe could be used very effectively in a cross-sectional scan. In addition, the high temperatures and long times required to attain the steady-state lead to extensive losses of tin from the copper-tin membranes.

A very interesting phenomenon, believed to be an enhanced Kirkendall effect in the grain boundaries is shown in the micrograph of Figure 16. This feature, which occurs in both binary and ternary systems, is a possible explanation for the appearance of cracks in the diffusion membrane since the high mobility of this grain boundary material could lead to a traversing of the entire membrane thickness.

Further investigation will be carried out when the McMaster Probe is operational.

These preliminary experiments served to illustrate that the steady-state experiment cannot be used successfully in the copper-zinc-tin ternary system because of the tin losses from the membrane. Investigation of infinite and finite couples was carried out therefore with the aim of producing a measureable off-diagonal effect.

ii) Infinite Couple Diffusion

Diffusion couples with semi-infinite boundary conditions were prepared for the evaluation of the four diffusion coefficients in the ternary system, D_{11}, D_{22}, D_{12}, and D_{21} as well as the two coefficients in the binary system, D_{11} and D_{22}, where tin is component 1 and zinc is component 2.

In the first experiment, designed to include the concentration range 0 to 5 atom percent zinc and 0 to 4.25 atom percent tin, the couples were welded in hydrogen for three hours and diffused in argon for 1.44×10^5 seconds (40 hrs) at $821.5 \pm 0.9^{\circ}C$. Concentration profiles were determined by point counting with the A.R.L. Probe in the Metallurgy Department at M.I.T., Cambridge, Mass. Diffusion coefficients were determined by Boltzmann-Matano analyses using Equation 7 for the on-diagonal coefficients and Equation 21 for the off-diagonal coefficients. The concentration profiles and calculated diffusion coefficients are shown in Figures 17 to 20.

Since D_{21} in Figure 19 was not measureable, the entire experiment was repeated using a larger initial concentration step in component one. The diffusion couples, prepared in the same way as above, were

diffused for 1.209×10^6 seconds (two weeks) at $497.7 \pm 0.4^{\circ}C$. The results obtained by continuous scanning with the A.M.R. Probe are shown in Figures 21 to 24.

iii) Finite Diffusion Couple with Reflection from a Boundary

The finite diffusion couples were prepared by welding thin alloy slabs together in hydrogen and diffusing these for 1.209×10^6 seconds at $497.7 \pm 0.4^{\circ}C$. The three alloy compositions used were: copper - 5.75 atom % tin, copper - 5.30% zinc and copper - 5.51% tin - 5.30% zinc.

In order to achieve the boundary conditions shown in Figure 3, multi-layer couples of the form CuZnSn-CuSn-CuZnSn-CuSn-CuZnSn-CuSn-CuZnSn were prepared where the end ternary alloys were thick slabs (infinite boundaries) and the five internal alloys were thin slabs with finite boundaries. In order to determine the other off-diagonal coefficient, similar couples were prepared by substituting CuZn for CuSn binary alloys.

For the diffusion time and temperature used, the optimum thickness of each of the five thin slabs (dimension L in Figure 3) was calculated to be 0.0027 inches from available diffusion data (23). To ensure the observation of the maximum effect despite uncertainty in the design data, couples with both zinc and tin step function distributions were prepared with slab thickness 0.0020, 0.0027 and 0.0034 inches in the hopes of bracketing the optimum test conditions.

Concentration profiles were obtained by continuous scanning with the A.M.R. Probe. The results for the 0.0027 and 0.0034 inch couples are shown in Figures 25 to 28. In Figure 25, the off-diagonal coefficients

were obtained by fitting Equation 45(a) to these curves. The off-diagonal coefficient in Figure 27 was calculated with the assumption of infinite boundary conditions using Equation 41.

From these diffusion data, values of the interaction parameter, ε_{12}, were calculated from Equations 34 and 35. Both the diffusion and thermodynamic results are tabulated in Table II.

DISCUSSION

The analysis of the infinite diffusion couple data was carried out using the Boltzmann-Matano analysis in the usual way for the on-diagonal coefficients. It was found that the determination of areas by counting squares, and with the planimeter, gave approximately the same precision. However in the past there has been some confusion (11) in the determination of off-diagonal coefficients using Equation 21. In evaluating the area, the total area either above or below the mean composition must be considered, since the independent variable in the integral is the concentration.

Although the analysis of the finite couple data is based on the very restrictive conditions that the diffusion coefficients must be nearly equal and independent of concentration, the much larger effects to be measured make possible a fairly accurate estimate of the off-diagonal coefficients. The data of Figure 25 (for the time, temperature, and couple dimensions used) fit Equation 45 very accurately for both components. In the wider couple of the same type shown in Figure 26, the zinc distribution did not correspond to Equation 45, indicating that the optimum time had not been reached for these couple dimensions. This result shows the necessity of preparing a number of finite couples to bracket the calculated optimum dimensions when the diffusion coefficients are not known accurately.

In the other type of finite couple shown in Figure 27 and 28, the zinc (originally uniform) diffuses more slowly than does the tin (initially with step distribution). In this case, perturbations occur in the zinc distributions at the points $\pm \xi$ (see Figure 3). The data shown in Figure 27 were analyzed by means of Equation 41. This simplified approach overcame the difficulties of fitting a series solution of the form given in Equation 45 to the experimental data. The resultant value of D_{21} would seem to be more accurate than that obtained by the Boltzmann-Matano analysis of the concentration profile of Figure 23 since the former results from the average of many perturbations of the zinc concentration while the latter arises from only one perturbation. In fact the Boltzmann-Matano analysis would appear to be an order of magnitude too low. This conclusion is borne out by the calculated ε_{12} values given in Table II.

The average grain size in the couples is indicated in Table II. At 821.5°C and with the large grain size, grain boundary diffusion will have little or no effect on the bulk diffusion coefficients. However, at the lower temperature (497.7°C) and with the smaller grain size, grain boundary diffusion may have some small effect on the diffusion coefficients measured. For this reason, it is important to state the grain size in diffusion studies although this information is often overlooked in the literature (23).

The importance of the choice of concentration units cannot be over-emphasized. In this thesis, atom percent was chosen because it gives a clearer microscopic picture of the diffusion process. In this system of units, fluxes can be expressed in terms of atoms jumping from

one plane to the next. Also the Matano interface, on each side of which the number of atoms remains constant, corresponds to the original weld position for all diffusion times provided distortion and porosity do not occur. When concentrations are measured in weight percent, the Matano interface position so determined is not related in a simple way to the original weld or to any inert markers placed in the original weld.

The conversion of diffusion coefficients measured in one unit system to those in another unit system has been stated by DeGroot and Mazur (24). Equation 12(a) is

$$\frac{\partial \rho_i}{\partial t} = J_i = -\sum_{k=1}^{n-1} D_{ik} \nabla C_k$$

if the concentrations C are measured in grams per cubic centimeter or gram moles per cubic centimeter. The equivalent expression in terms of mole fraction (or atom percent) subject to dilute solution approximation, ie. $N_i << 1$ for i = 1, 2, ---n-1 and $N_n \simeq 1$, is

$$\frac{\partial N_i}{\partial t} = J_i = \sum_{k=1}^{n-1} \frac{M_k}{M_i} D_{ik} \nabla N_k$$

where M_k is the gram molecular weight of the kth component. It is obvious from this expression that care must be taken in converting from one unit system to another, especially in the case of off-diagonal coefficients.

The evaluation of the probable error in the experimentally measured coefficients poses a problem which is not easily soluble. A summation of the errors in diffusion time and temperature amounts to only a small fraction of the probable error.

In the case of on-diagonal coefficients, a large error is introduced in drawing the tangents to the experimental curves. As can be seen from Figure 24a in which the counting statistics are shown, a possible error of 10 percent could be introduced in the intercept due to the undertainties in drawing the tangents to this curve at the Matano interface. Since the intercept distance is sqared in the calculation of the diffusion coefficient, a possible error of 20 percent is introduced. In order to obtain a reliable standard deviation for the diffusion coefficients, the experiment should be repeated several times and the tangents in each case should be drawn by several people in order to obtain a statistical average. Since the time and money were not available for repetition of the experiment, onecan only estimate the probable accuracy of the results. The diffusion coefficients listed in Table II are considered by the author to be the most probable values but a possible error of plus or minum 25 percent must be considered.

In the determination of the off-diagonal coefficients, an even greater probable error exists. Because the effect to be measured is small in the best possible cases, any estimate is inherently inaccurate. Again the author has given in Table II what he considers to be the most probable values but the correct result could differ by 50 percent from these numbers.

The errors in diffusion coefficients are reflected in the activation energy (Q) values listed in Table II.

However, one must keep in mind that the purpose of this investigation was to determine the degree of enhancement to be expected with various couple designs rather than to make very accurate diffusion coefficient measurements.

CONCLUSIONS

1. All of the diffusion coefficients in the dilute range of this system show strong concentration dependence.
2. The presence of the third element greatly enhances the binary on-diagonal diffusion coefficients as can be seen by the change in activation energies.
3. When the on-diagonal diffusion coefficients are approximately equal, the measureability of the off-diagonal effect is greatly moderated.
4. The initial concentration step in the infinite couple must be large to observe a cross-effect.
5. The finite couple is more effective in producing a measureable cross-effect than is the infinite couple.
6. Tin increases the thermodynamic activity of zinc in copper.

BIBLIOGRAPHY

1. Bareham, F.R. and Fox, J.G.M., J. Inst. Metals 88(8), 344, (1959).
2. Castaing, R. and Guinier, A., Anal. Chem. 25, 724, (1953).
3. Fick, A., Pogg. Ann. 94, 59, (1855).
4. Boltzmann, L., Ann. Physik, Leipzig, 53, 959, (1894).
5. Gosting, L.J. and Fujita, H., J. Am. Chem. Soc. 78, 1099, (1956).
6. Crank, J., Mathematics of Diffusion, Oxford University Press, London, (1957).
7. Matano, C., Japan J. Phys. 8, 109, (1933).
8. Smigelskas, A.D. and Kirkendall, E.O., Trans. A.I.M.E. 171, 130, (1947).
9. Onsager, L., Ann. N.Y. Acad. Sci. 46, 241, (1945).
10. Kirkaldy, J.S., Can. J. Physics 35, 435, (1957).
11. Mason, G.R., M. Eng. Thesis, McMaster University, (1959).
12. Weichert, D.H., M.Sc. Thesis, McMaster University, (1963).
13. Kirkaldy, J.S., Zia-Ul-Haq, and Brown, L.C., Submitted to A.S.M. Trans. Quarterly, (1963).
14. Kirkaldy, J.S., Can. J. Physics 36, 899, (1958).
15. Darken, L.S., Trans. A.I.M.E. 180, 430, (1949).
16. Kirkaldy, J.S., Trans. A.S.M. 55, 998, (1962).
17. Darken, L.S., A.S.M. Trans. 43A, 1, (1951).
18. Kirkaldy, J.S. and Purdy, G.R., Can. J. Phys. 40, 208, (1962).
19. Duane, W. and Hunt, F.L., Phys. Rev. 6, 166, (1915).

20. Powers, M.C., X-Ray Spectrometer Conversion Tables for Topaz, LiF, NaCl, EDDT, and ADP Crystals, Philips Electronic Instruments, Mt. Vernon, N.Y.

21. Castaing, R., Ph.D. Thesis, Univ. of Paris, (1951).

22. Yue, A.S., and Guy, A.G., Trans. A.I.M.E. 212(1), 107, (1958).

23. Smithells, C.J., Metals Reference Book, Vol. 1, Butterworth Scientific Publications, London, (1955).

24. DeGroot, R.S., and Mazur, P., Non-Equilibrium Thermodynamics, North-Holland Publishing Co., Amsterdam, Pg. 261, (1961).

Sample Number	Weight Percent Zinc	Atom Percent Zinc	Weight Percent Tin	Atom Percent Tin
1	0	0	0	0
2	2.19	2.13	0	0
3	4.98	4.85	0	0
4	0	0	3.25	1.77
5	2.57	2.53	2.98	1.62
6	5.34	5.27	2.92	1.59
7	0	0	7.45	4.13
8	2.45	2.46	6.80	3.77
9	5.00	5.04	7.56	4.20
10	0	0	11.40	6.44
11	3.03	3.10	10.40	5.86
12	6.26	6.36	10.30	5.76

TABLE I

Compositions of Calibration Standards

Couple No.	System (Sn = 1) (Zn = 2)	Temp (^{o}C)	D_{ii} $\frac{cm^2}{sec}$	Concentration for D_{ii} (atom percent)		D_{ik} $\frac{cm^2}{sec}$	Concentration for D_{ik} (atom percent)	Couple Type	Average Grain Size (mm)
1	Cu-CuZn	821.5 ± 0.9	$D_{22} = 4.9 \times 10^{-10}$	$C_1 = 0$	$C_2 = 2.30$				
2	Cu-CuSn		$D_{11} = 2.1 \times 10^{-9}$	$C_1 = 2.25$	$C_2 = 0$				
3	CuSn-CuZnSn		$D_{22} = 2.6 \times 10^{-9}$	$C_1 = 3.05$	$C_2 = 4.00$	$D_{12} = 7.5 \times 10^{-10}$ $D_{12} = 9.8 \times 10^{-10}$	$C_1 = 3.85$ $C_1 = 4.28$	Infinite	0.3
4	CuZn-CuZnSn		$D_{11} = 2.7 \times 10^{-9}$	$C_1 = 2.25$	$C_2 = 5.25$	Not Measureable			
5	Cu-CuZn	497.7 ± 0.4	$D_{22} = 7.5 \times 10^{-14}$	$C_1 = 0$	$C_2 = 2.08$				
6	Cu-CuSn		$D_{11} = 3.0 \times 10^{-12}$	$C_1 = 3.75$	$C_2 = 0$				
7	CuSn-CuZnSn		$D_{22} = 2.4 \times 10^{-12}$	$C_1 = 5.90$	$C_2 = 2.75$	$D_{12} = 4.6 \times 10^{-12}$ $D_{12} = 5.3 \times 10^{-12}$	$C_1 = 5.38$ $C_1 = 6.59$	Infinite	0.05
8	CuZn-CuZnSn		$D_{11} = 8.3 \times 10^{-12}$	$C_1 = 3.70$	$C_2 = 5.50$	$D_{21} = 2.9 \times 10^{-13}$	$C_2 = 5.64$		
9	CuSn-CuZnSn	497.7 ± 0.9				$D_{12} = 4.6 \times 10^{-12}$	$C_1 = 5.75$		
10	CuZn-CuZnSn					$D_{21} = 4.0 \times 10^{-12}$	$C_2 = 5.30$	Finite	0.05

Evaluation According to $D_{ii} = D_o e^{-Q/RT}$		D_o $\frac{cm^2}{sec}$	Q (Kcal)	Couples	ε_{12}
Couples	1 and 5	1.2	48.1	3 & 4 (D_{12} / D_{11})	+ 6.2
	2 and 6	1.3×10^{-2}	34.0	7 & 8 (D_{12} / D_{11})	+ 9.3
	3 and 7	3.6×10^{-2}	36.3	7 & 8 (D_{21} / D_{22})	+ 1.2
	4 and 8	2.7×10^{-3}	30.0	7 &10 (D_{21} / D_{22})	+ 7.8

TABLE II Tabulation of Diffusion and Thermodynamic Data

$$D(C) = \frac{-\frac{1}{2}\int_{C'}^{C} \lambda dC}{\left.\frac{dC}{d\lambda}\right|_C}$$

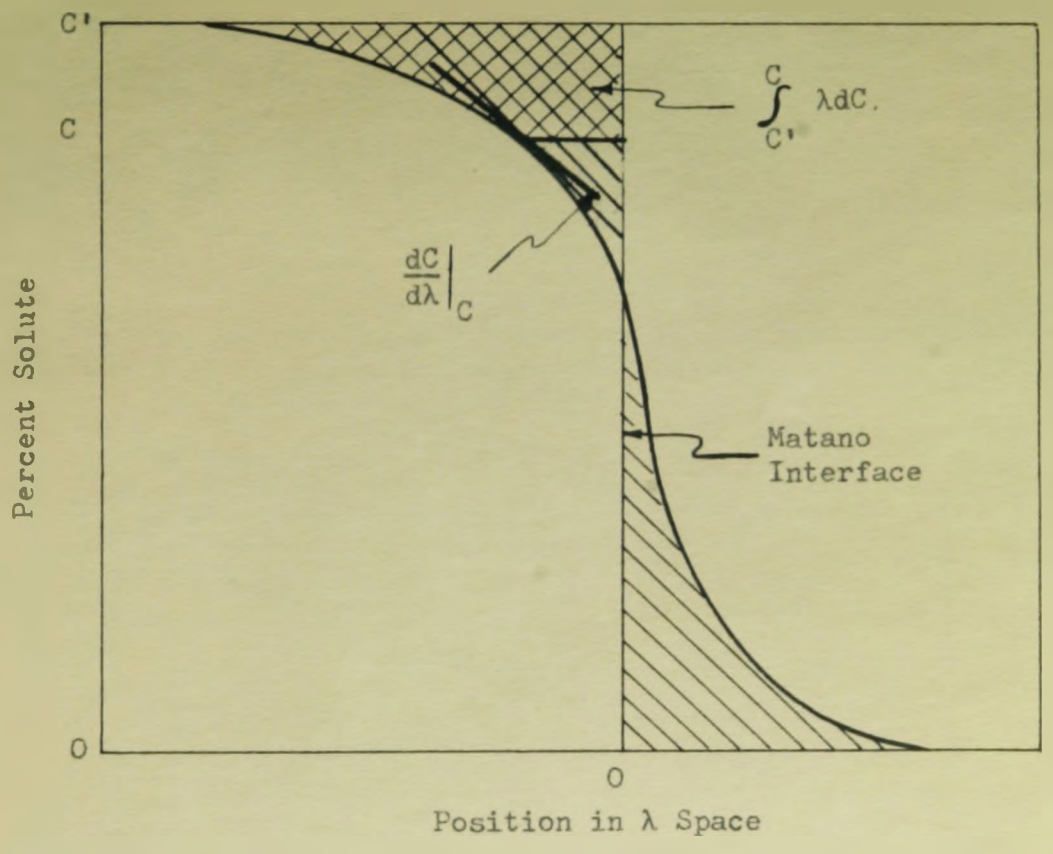

Figure 1 Typical Penetration Curve for Concentration-Dependent Coefficients in a Binary System

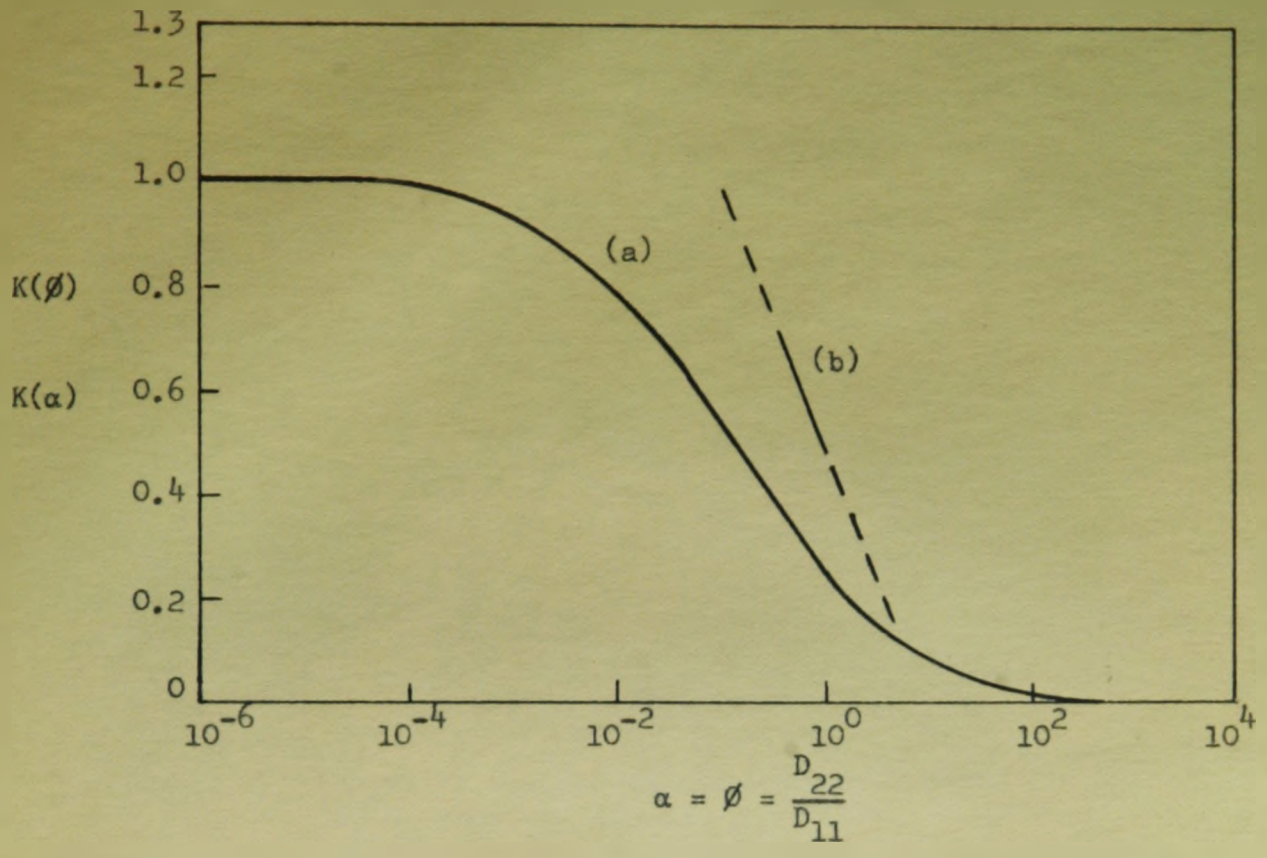

Figure 2 Theoretical Curves for the Variation of (a) K(Ø) in an Infinite Couple and (b) K(α) in a Finite Couple as a Function of D_{22}/D_{11}.

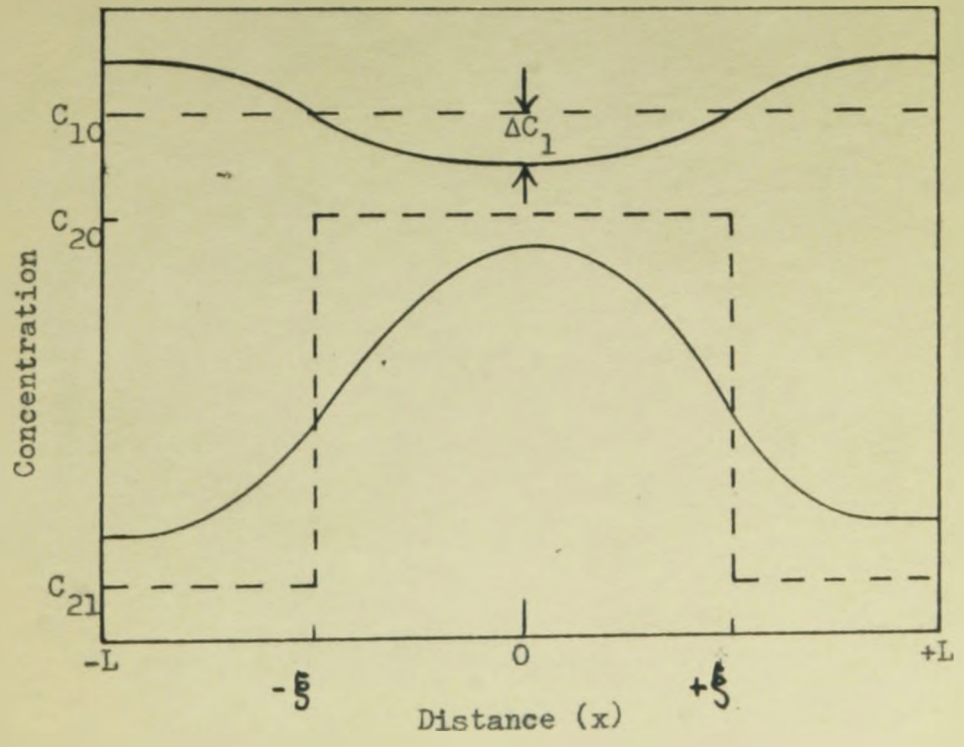

Figure 3 Schematic Representation of Concentration Profile at t=0 (dashed) and t=t (full) in a Finite Diffusion Couple with Reflection at the Boundaries $x = \pm L$.

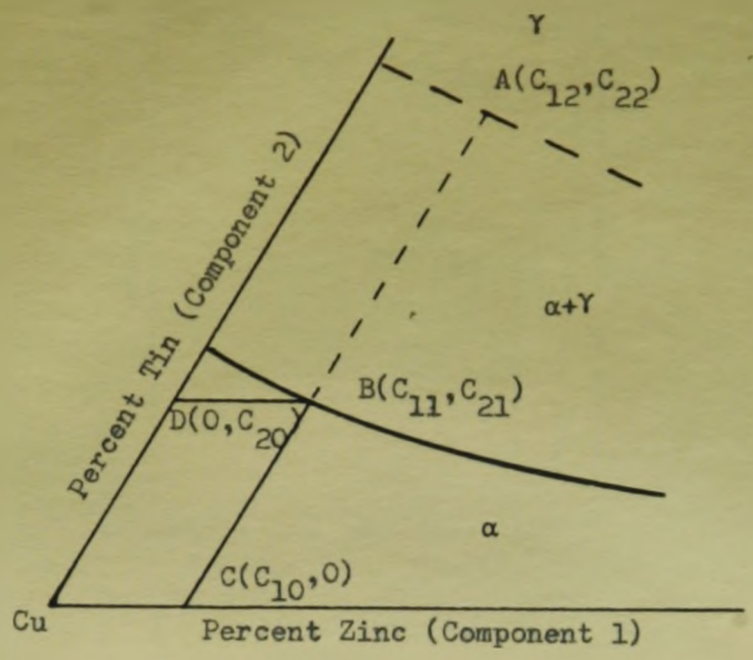

Figure 4 Schematic Diagram of the Copper-Zinc-Tin Isotherm at 500°C. showing tie line A·B.

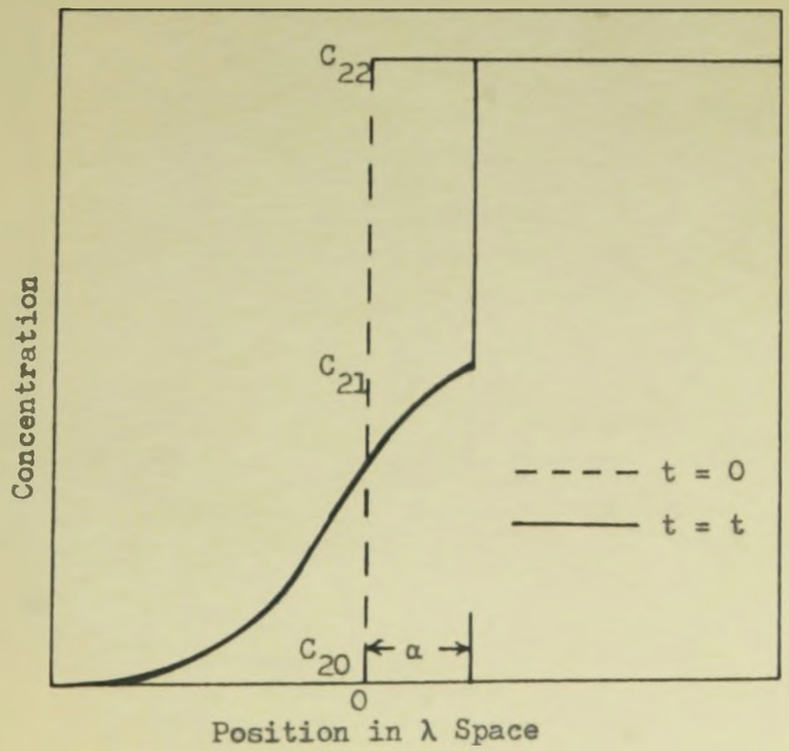

Figure 5 Schematic Diagram of Concentration Profiles in a Two Phase Couple at t=0 (dashed) and t=t (full)

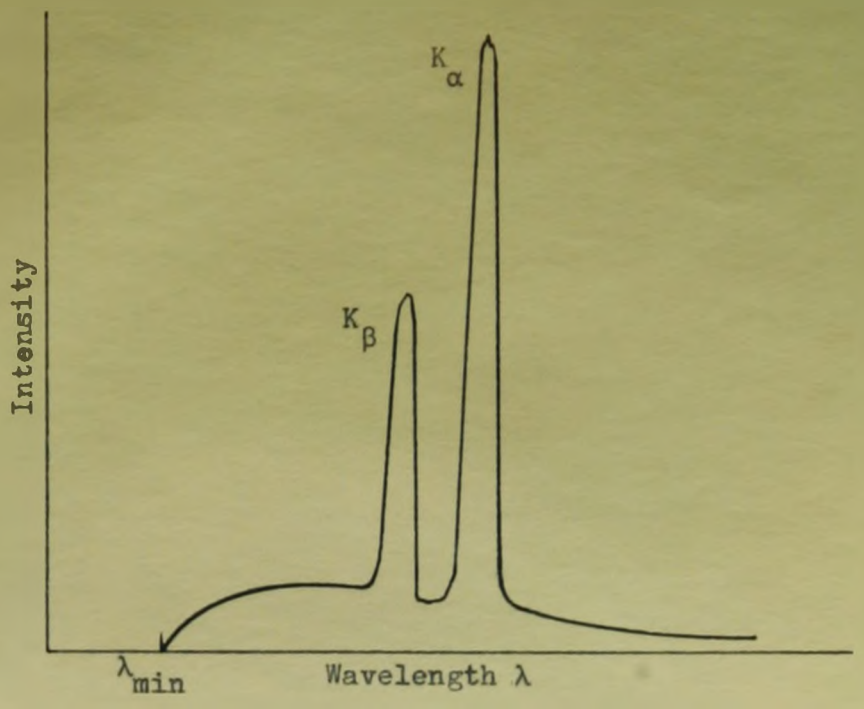

Figure 6 The Characteristic K Series Superposed on the Continuous Spectrum with Cut-off at λ_{min}

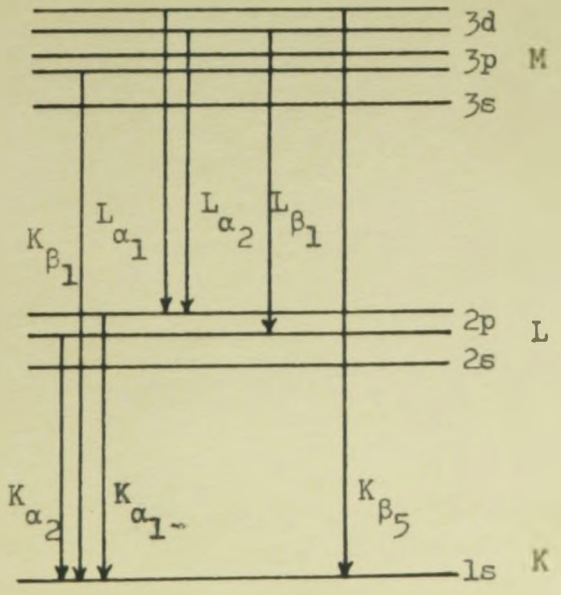

Figure 7 Diagram of the Most Probable Electron Transitions in the Inner Electron Shells of a Heavy Atom.

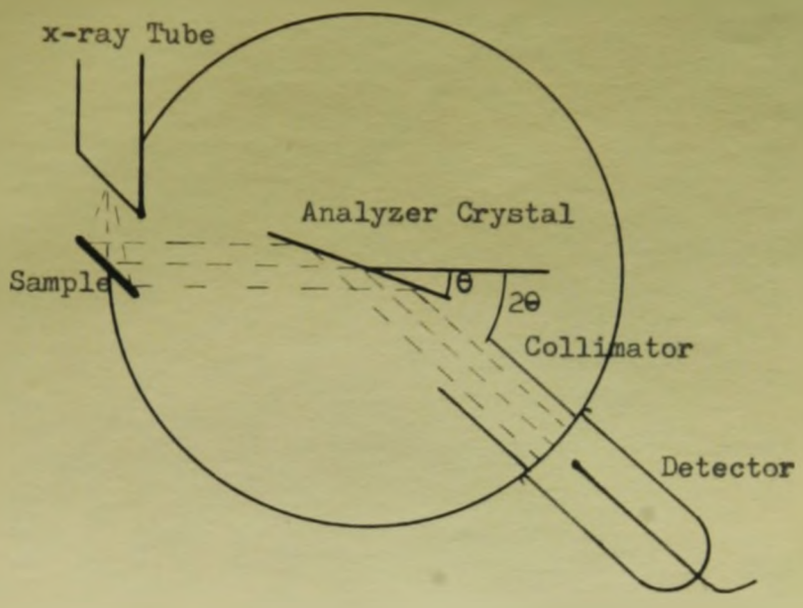

Figure 8 Simplified Representation of the X-ray Path in a Flat Crystal Dispersive System.

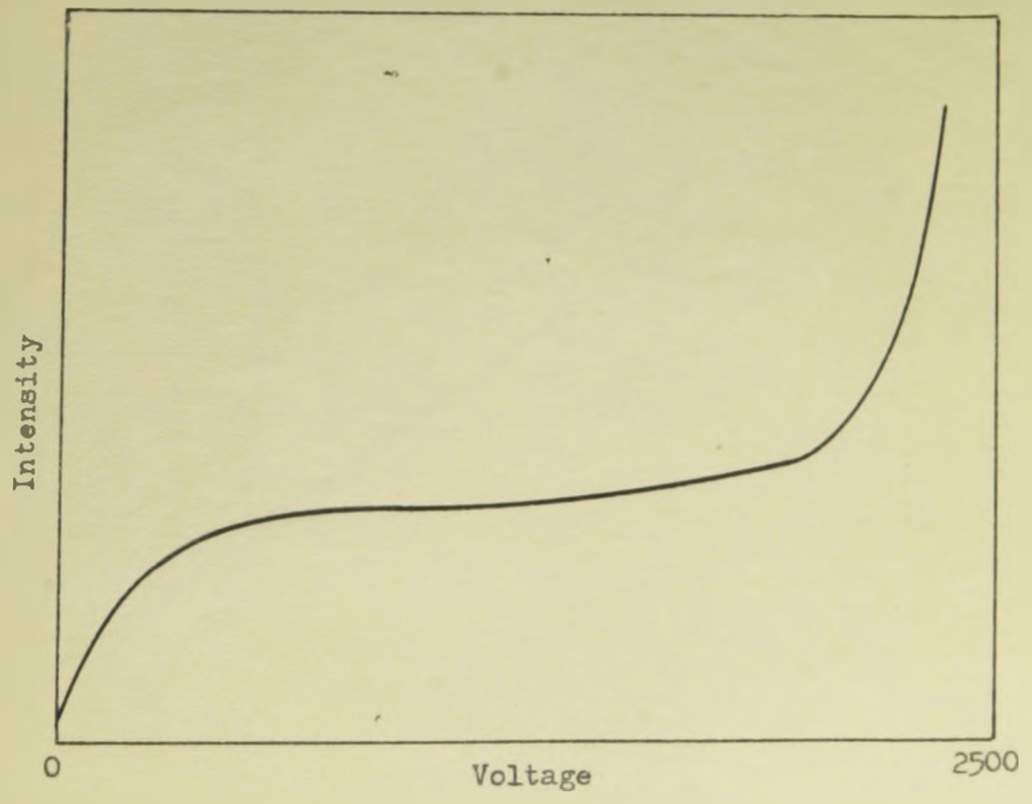

Figure 9 High Voltage Characteristics of the Scintillation Counter.

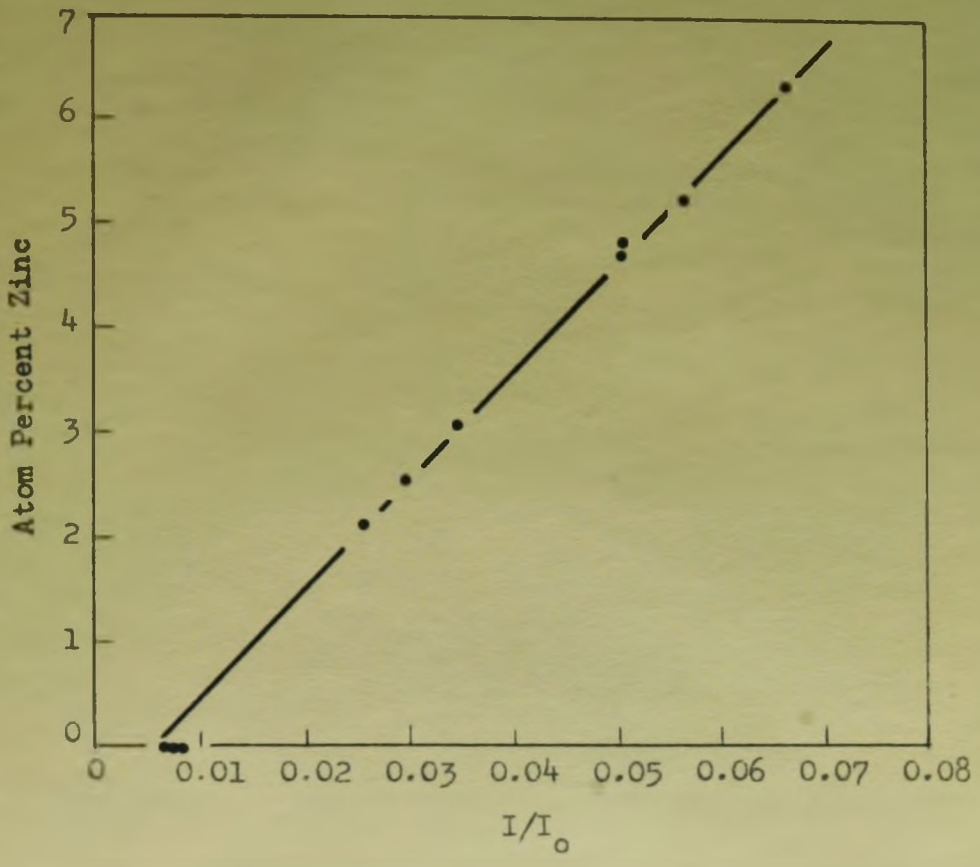

Figure 10 Calibration Curve for Zinc in Fluorescent Spectrometer on Zn K_{β_1} Line.

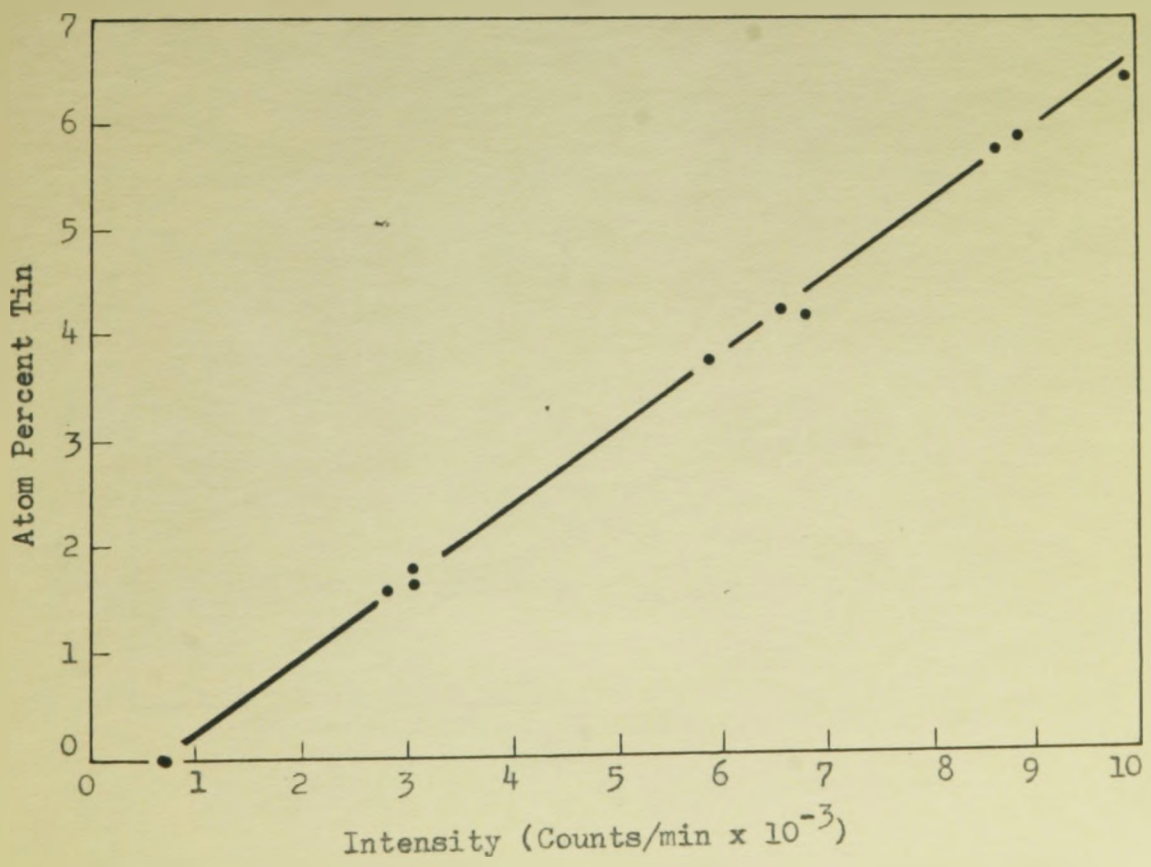

Figure 11 Calibration Curve for Tin in Fluorescent Spectrometer on Sn K_{α_1} Line.

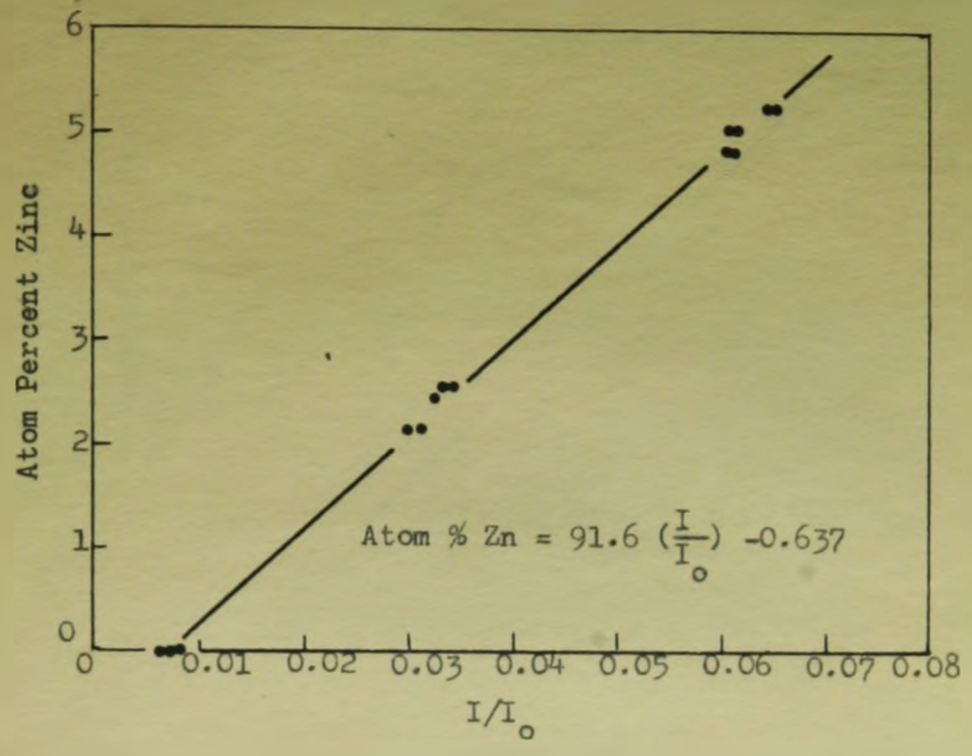

Figure 12 Calibration Curve for Zinc in A·R·L Probe (Take-off angle 52.5°) on Zn K_α (5th) Line at 30 KV.

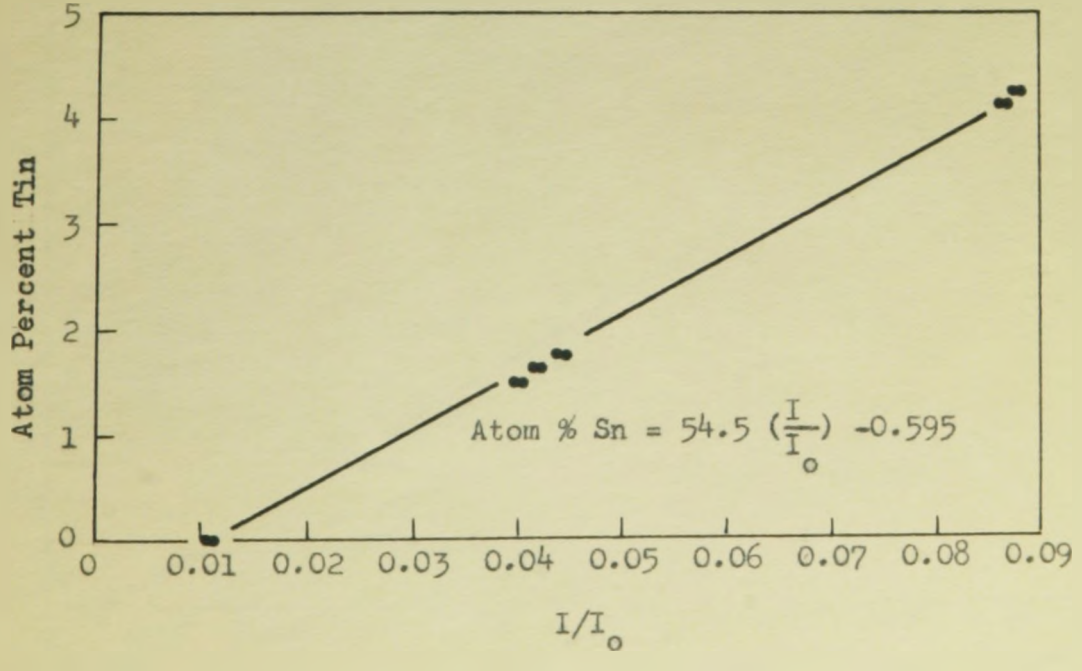

Figure 13 Calibration Curve for Tin in A·R·L Probe (Take-off angle 52.5°) on Tin L_α (3rd) Line at 30 KV.

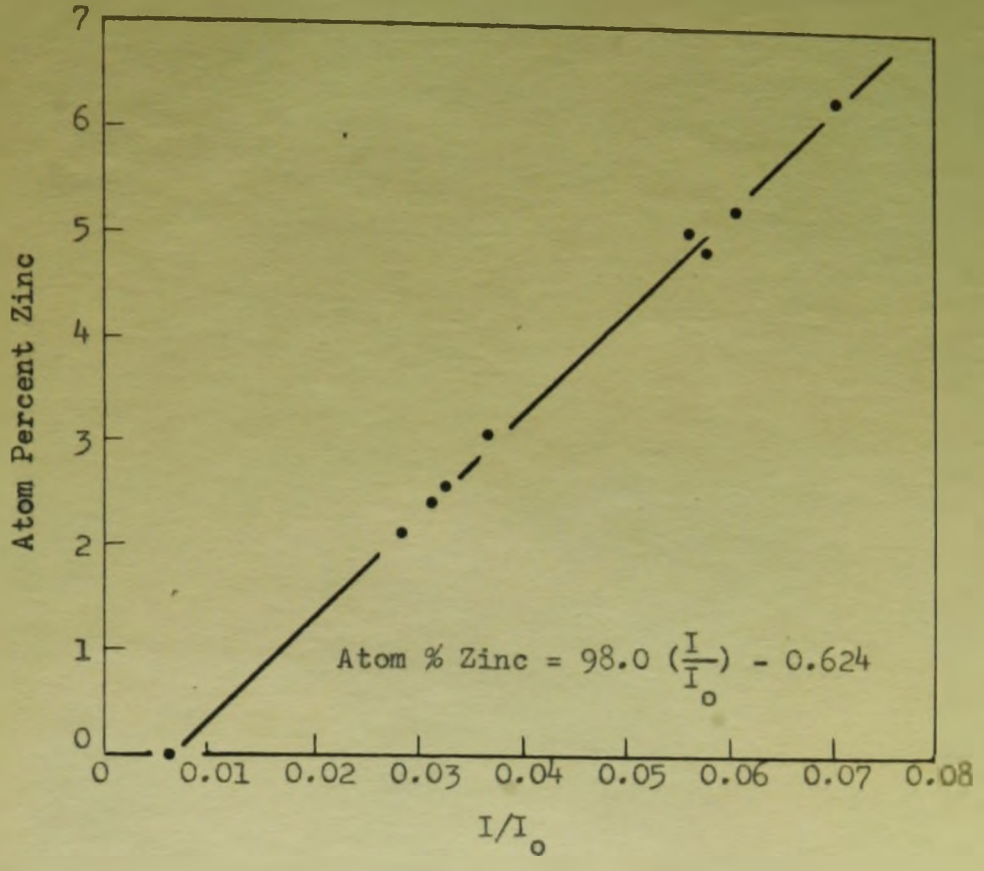

Figure 14 Calibration Curve for Zinc in A.M.R. Probe (Take-off angle 15.5°) on Zn K_α (5th) Line at 30 KV.

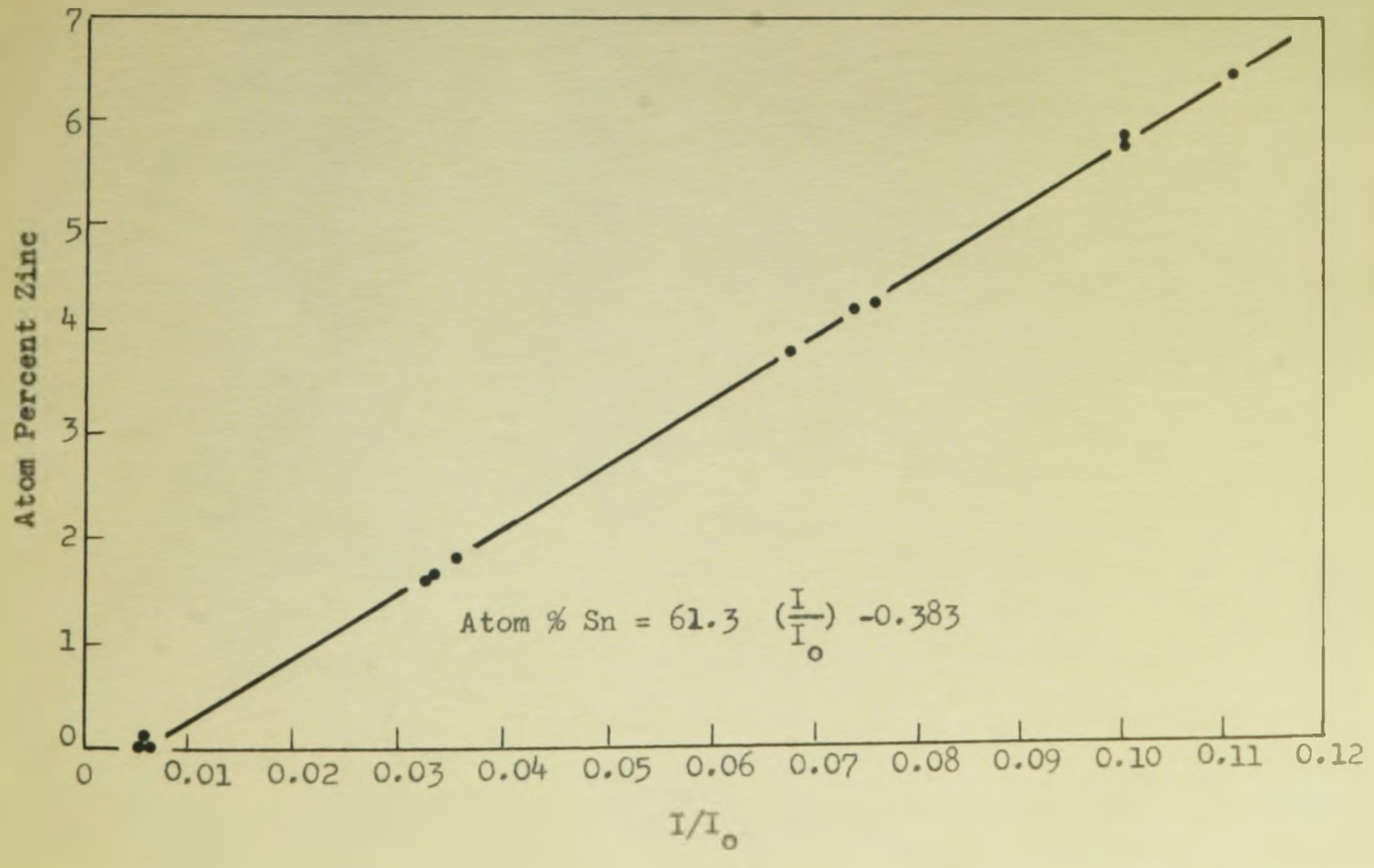

Figure 15 Calibration Curve for Tin in A.M.R. Probe (Take-off angle 15.5°) on Sn L_α (5th) Line at 30 KV.

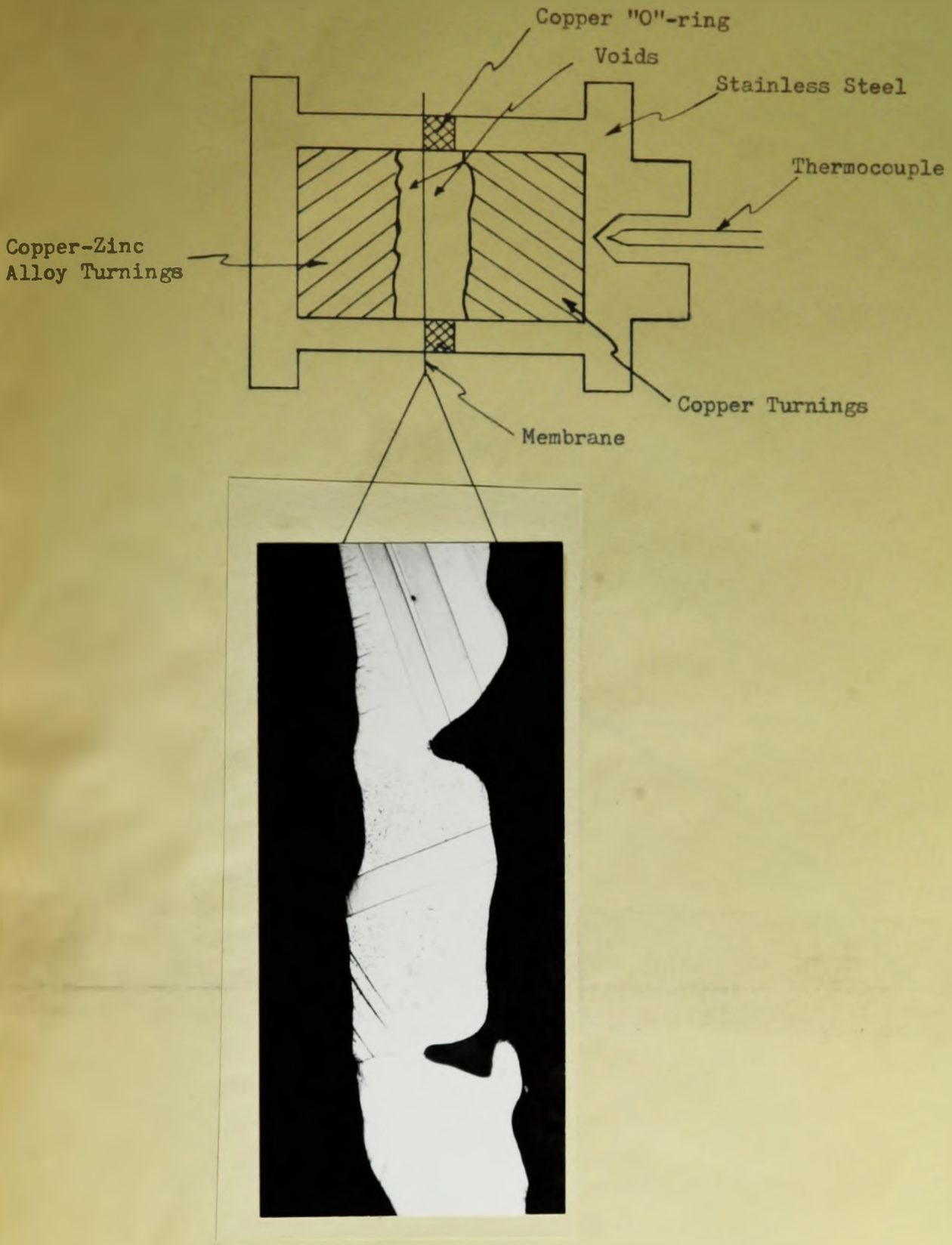

Figure 16 **Steady-State Diffusion Cell (actual size)** and Micrograph of a Diffusion Membrane when the Steady-State was Attained (X144).

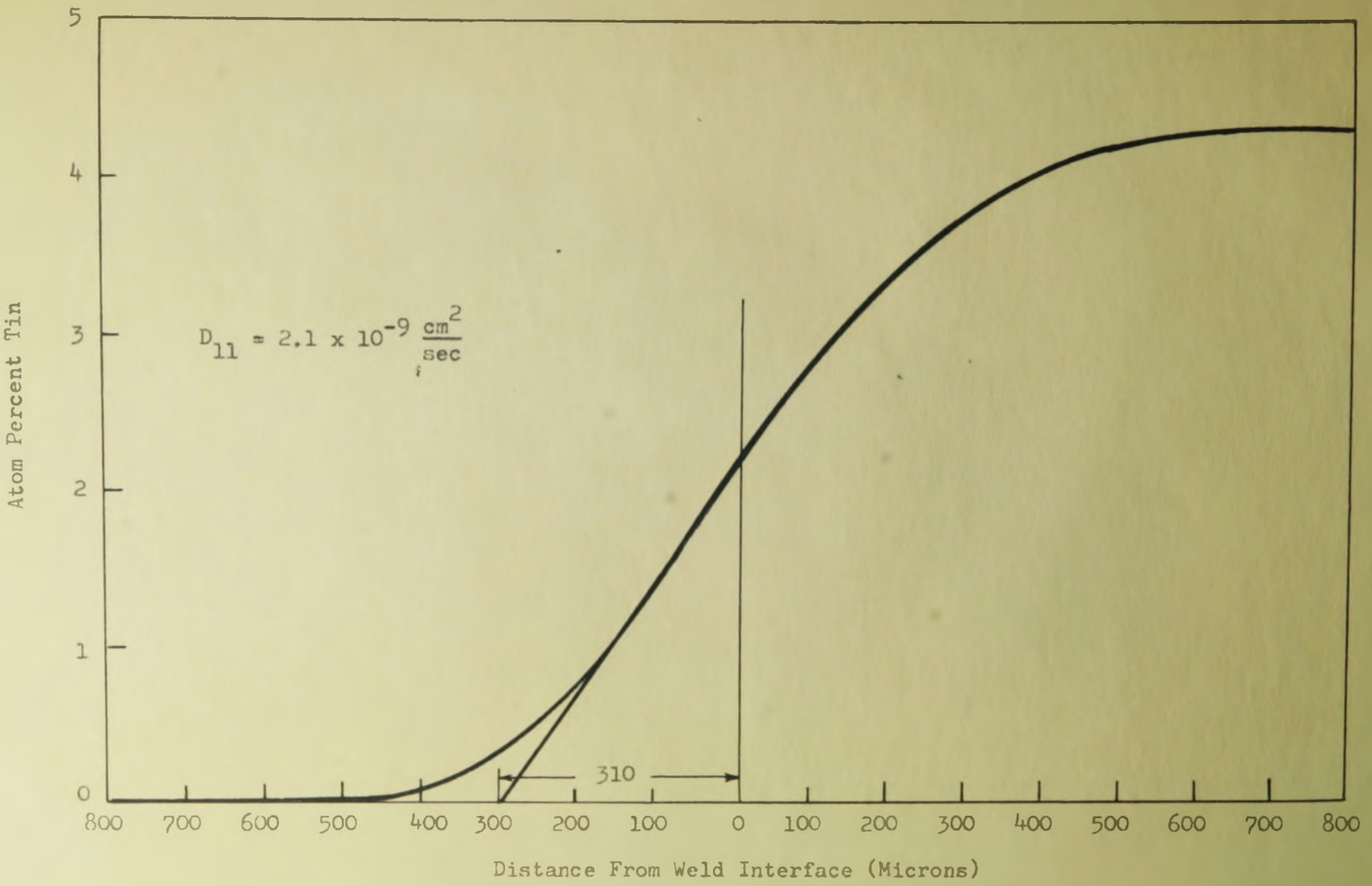

Figure 17 Concentration Profile in Cu-Cu Sn Couple

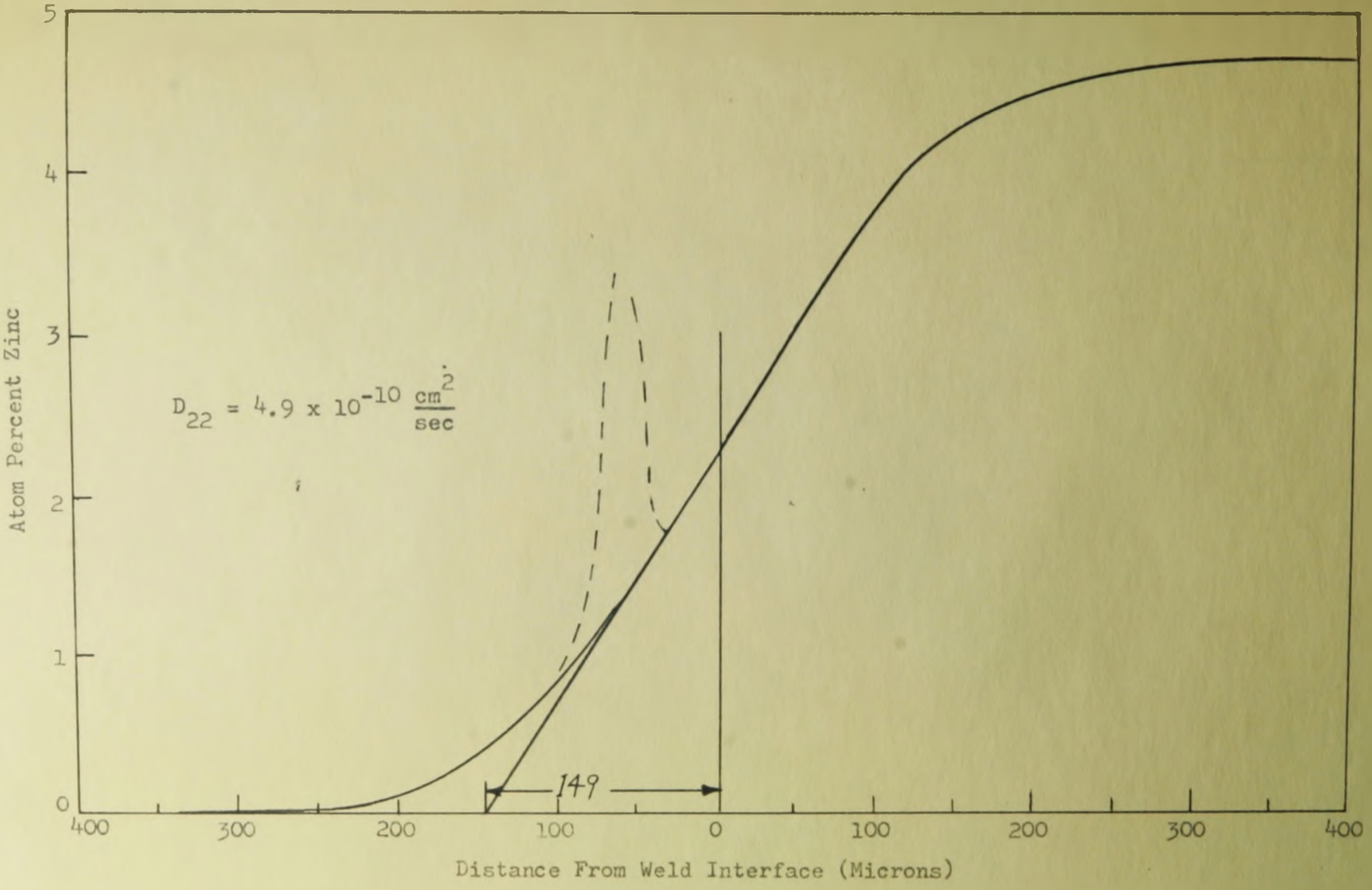

Figure 18 Concentration Profile in Cu - Cu Zn Couple

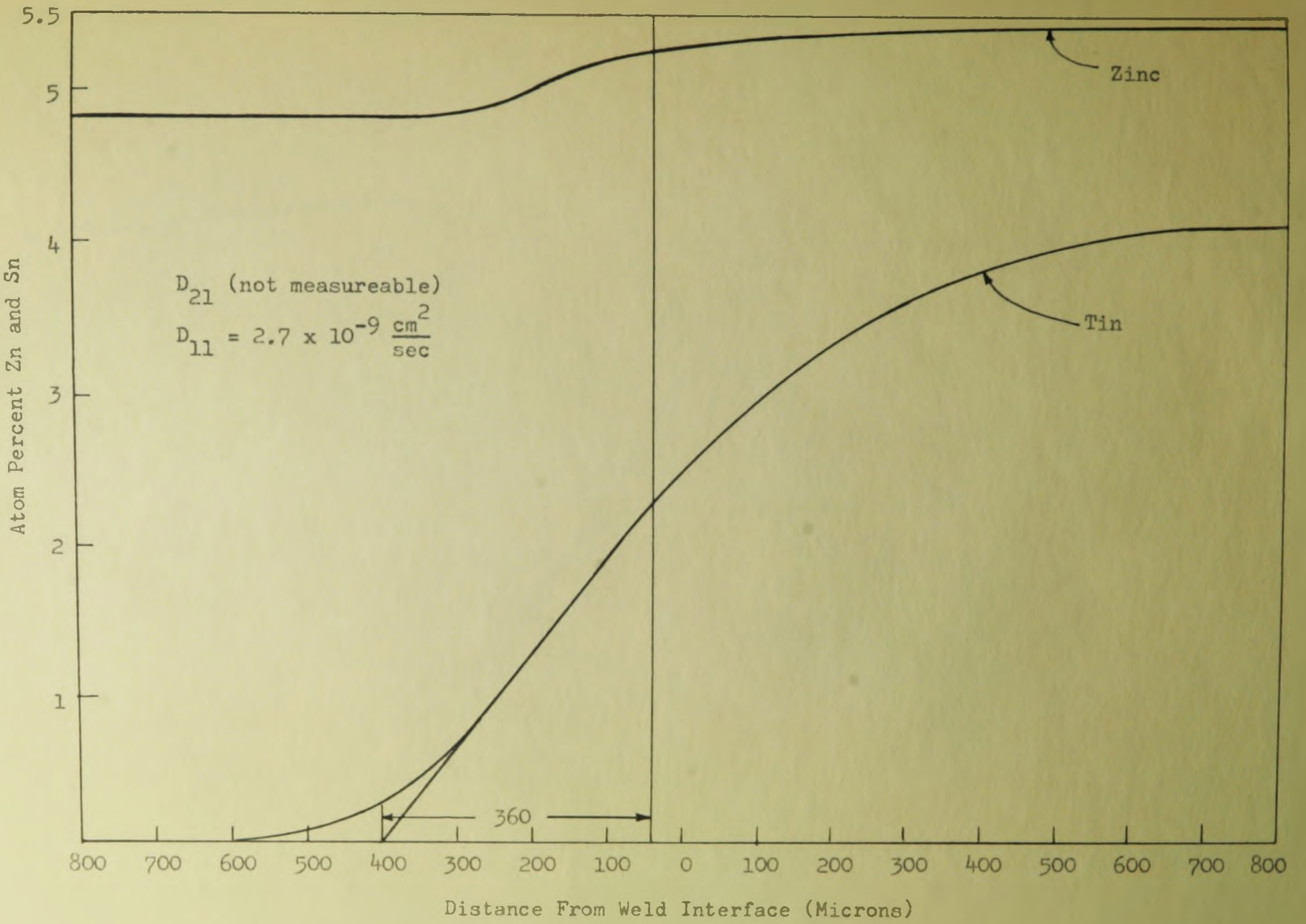

Figure 19 Concentration Profiles in Cu Zn - Cu Zn Sn Couple

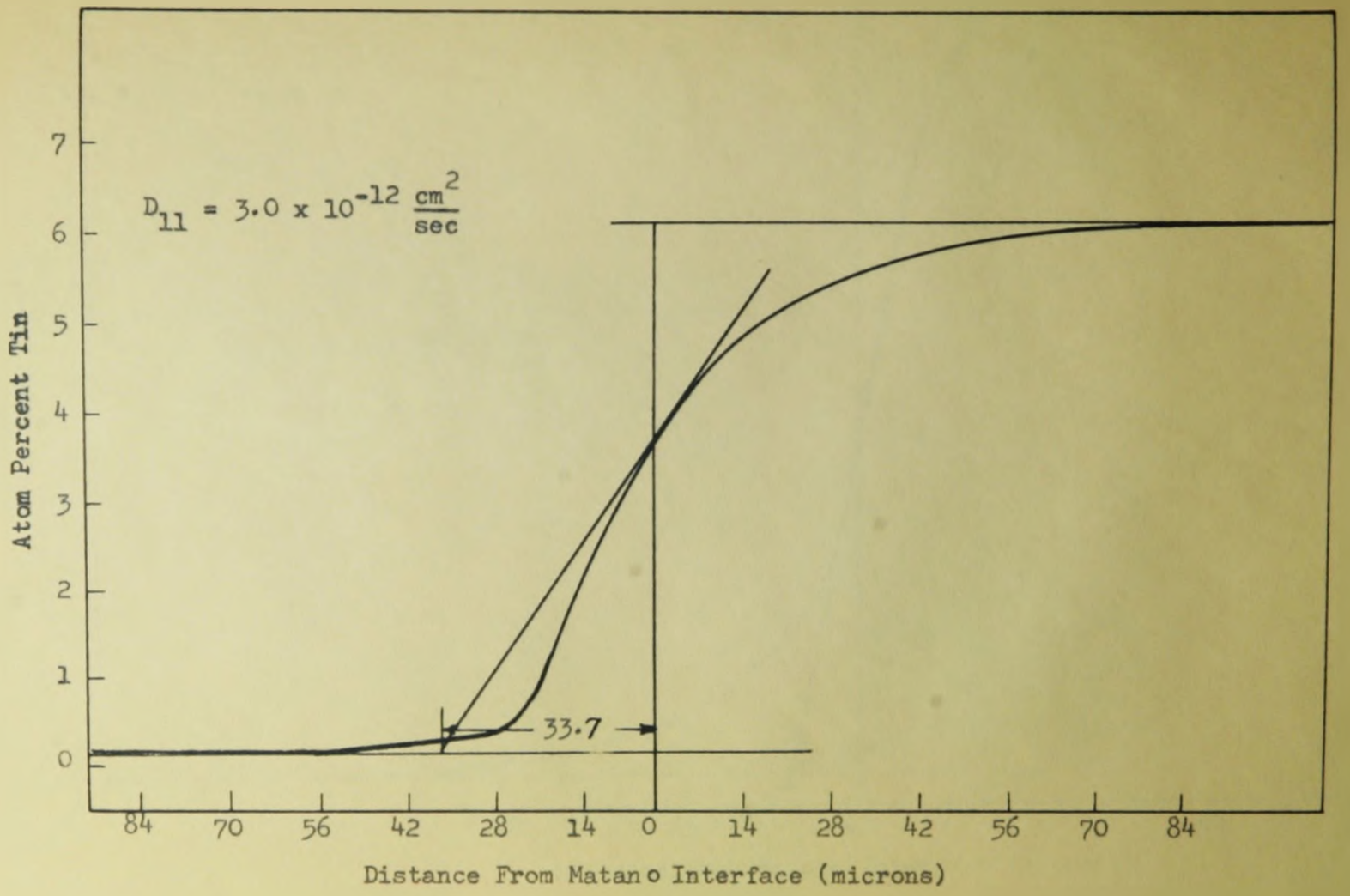

Figure 21 Concentration Profile in Cu - Cu Sn Couple

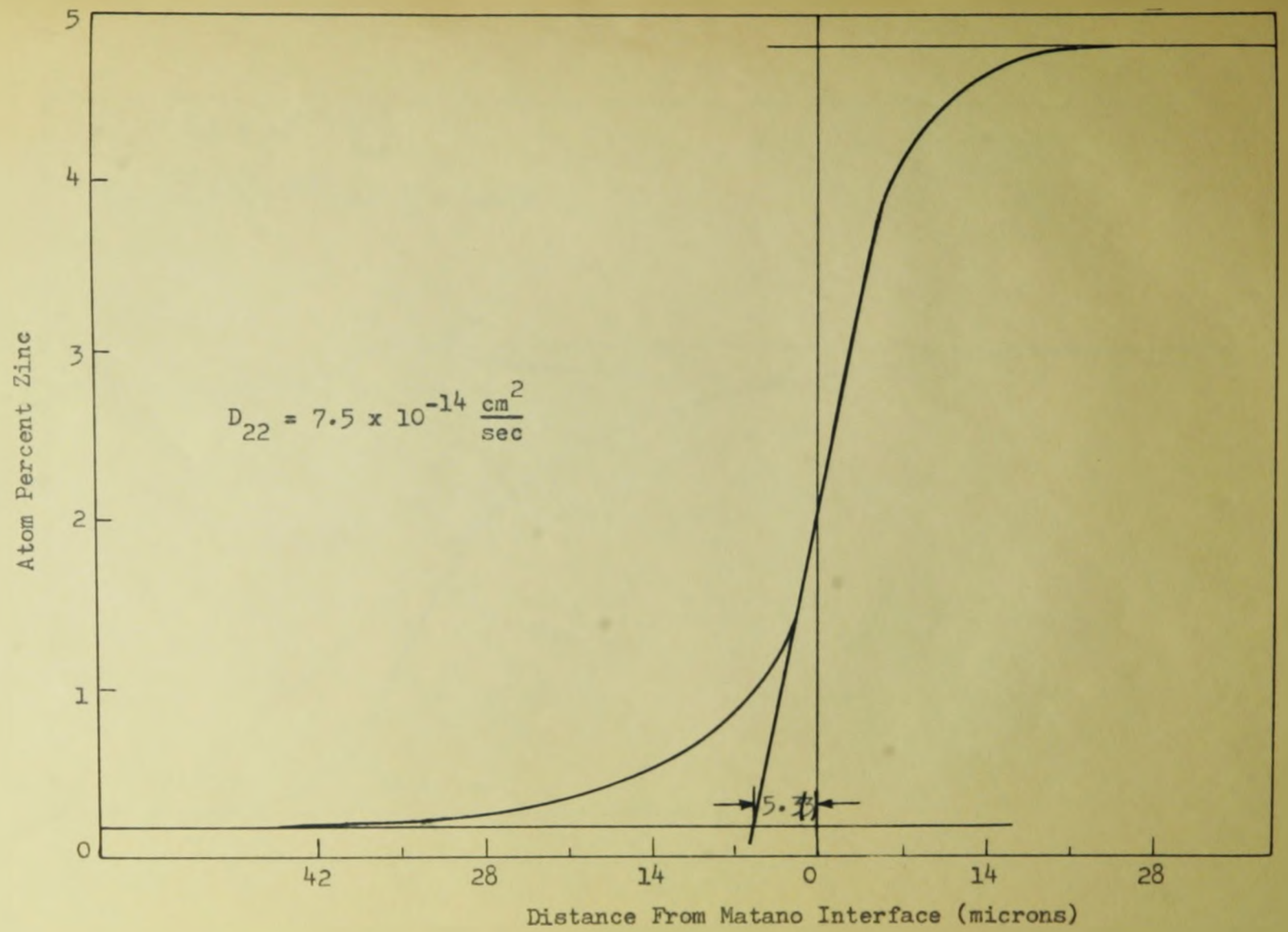

Figure 22 Concentration Profile in Cu-Cu Zn Couple

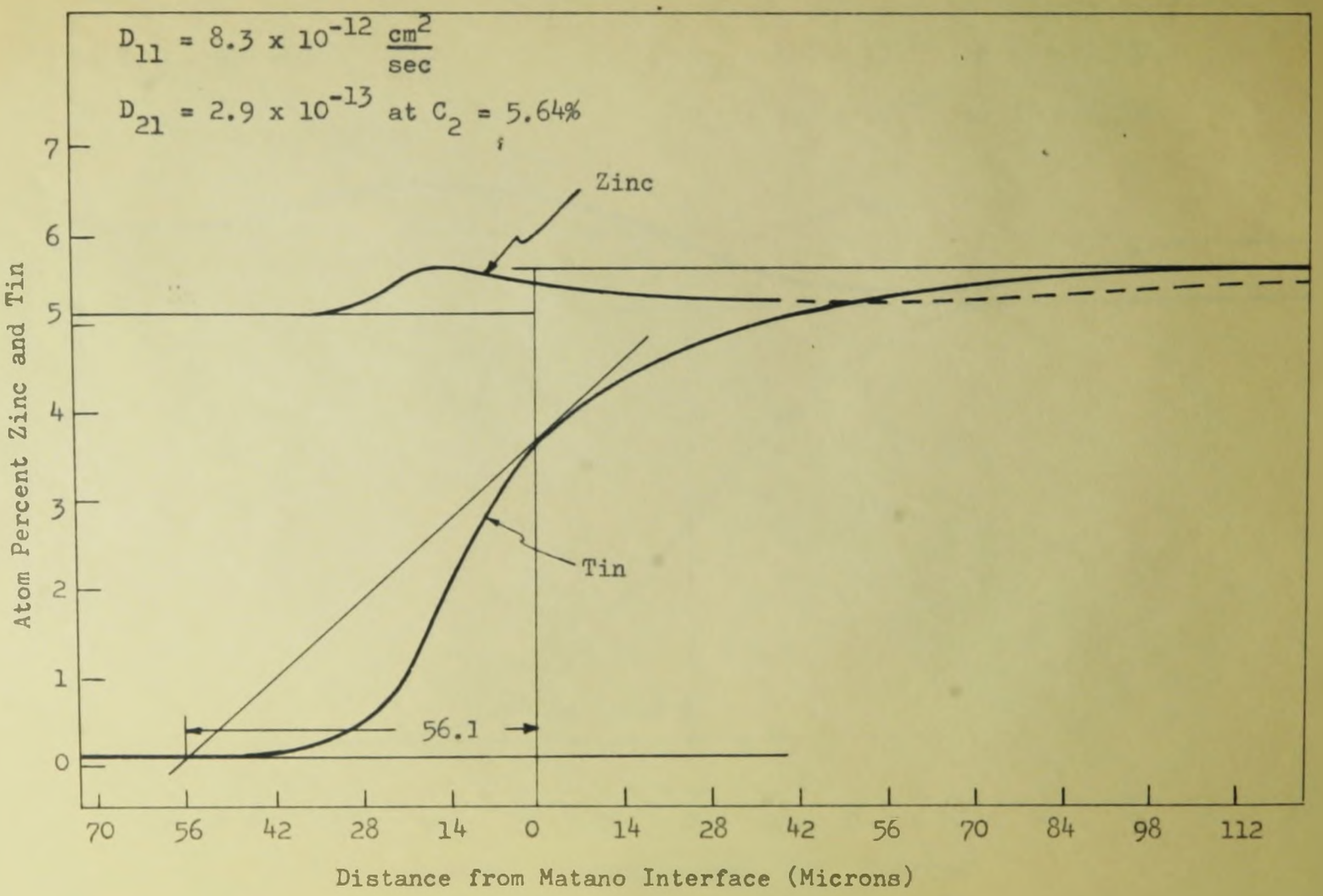

Figure 23 Concentration Profiles in Cu Zn - Cu Zn Sn Couple

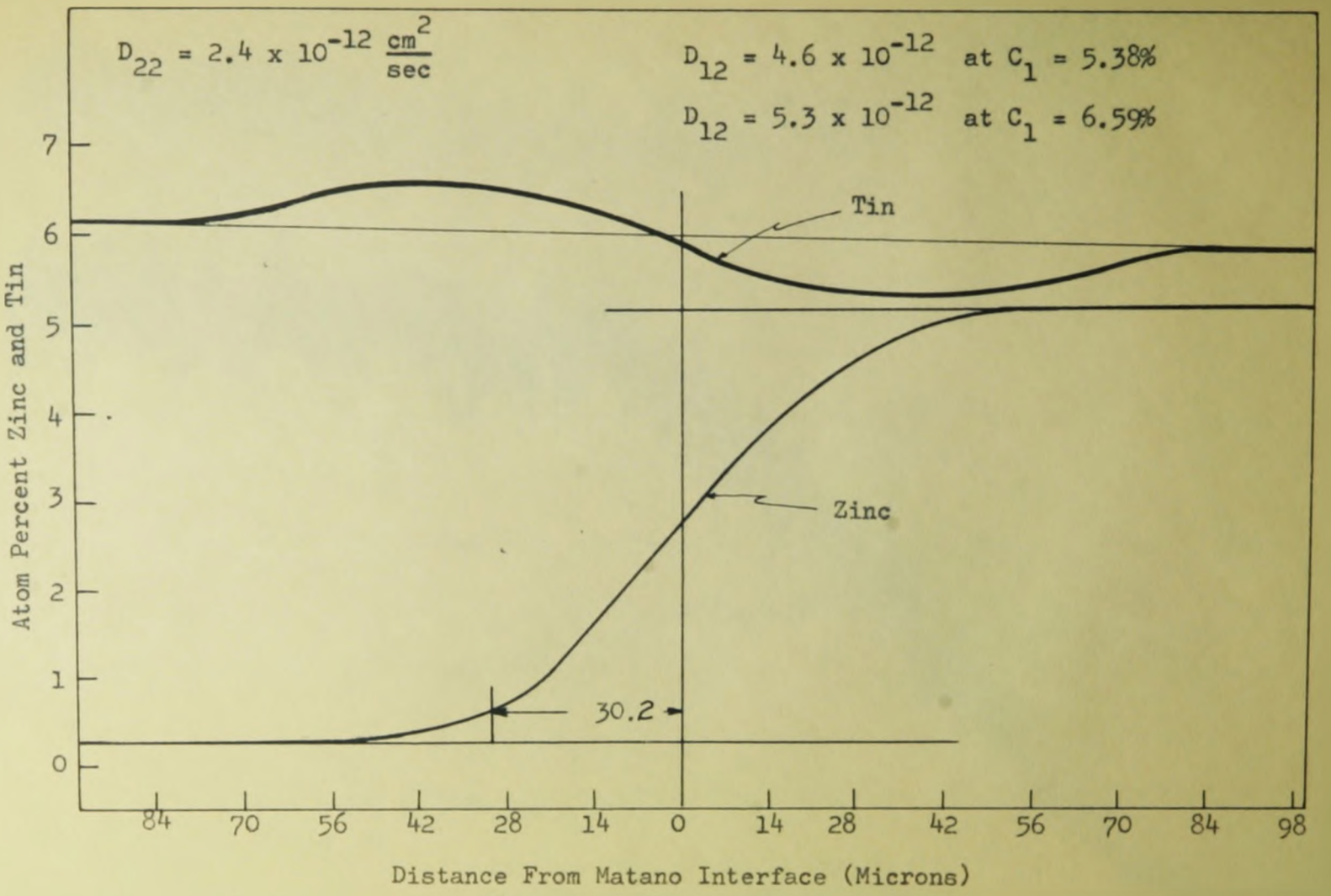

Figure 24 Concentration Profiles in Cu Sn - Cu Zn Sn Couple

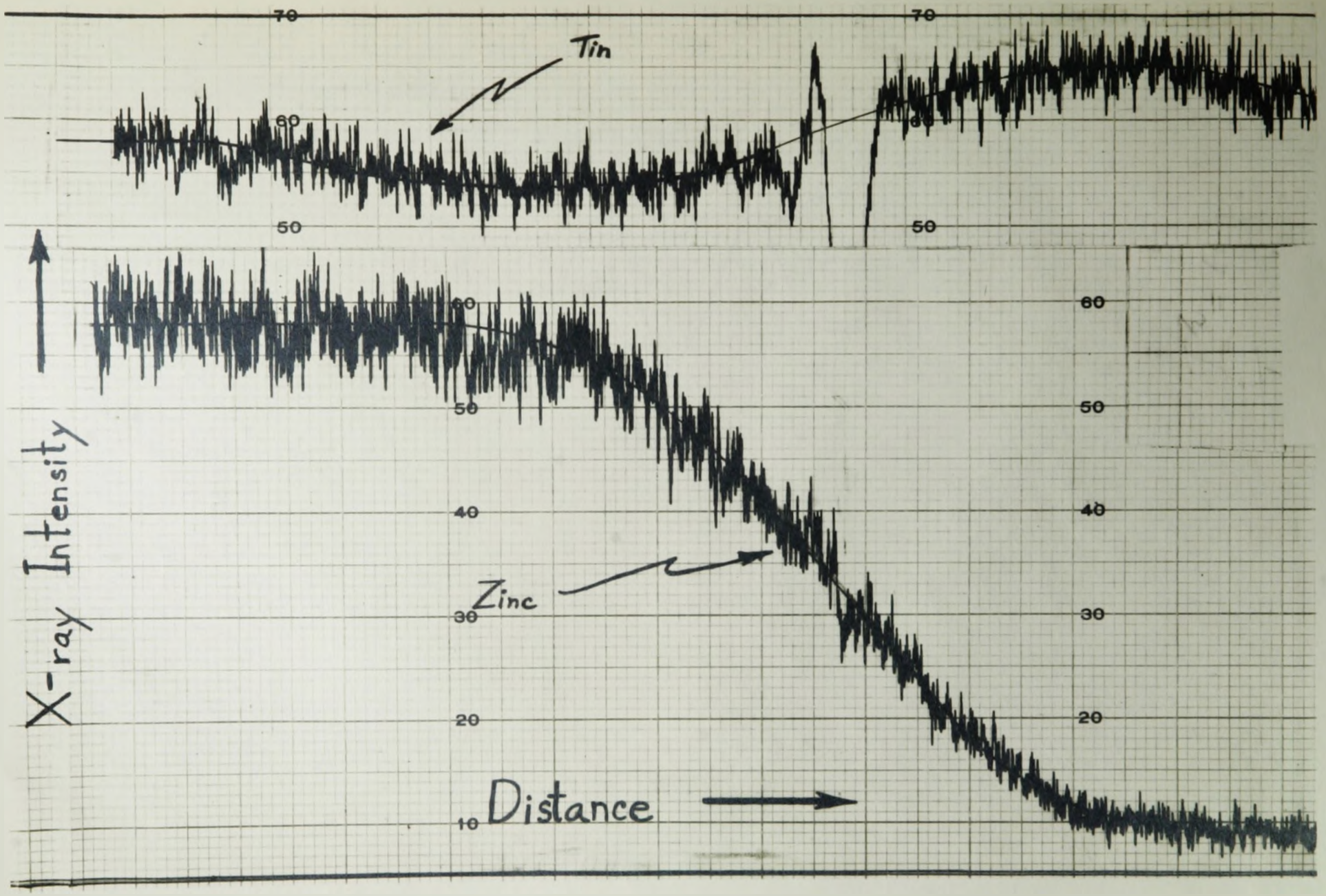

Figure 24a. Reproduction of Strip Chart from A.M.R. Probe Showing the X-ray Intensity Versus Distance from which the Penetration Curves of Figure 24 were Obtained.

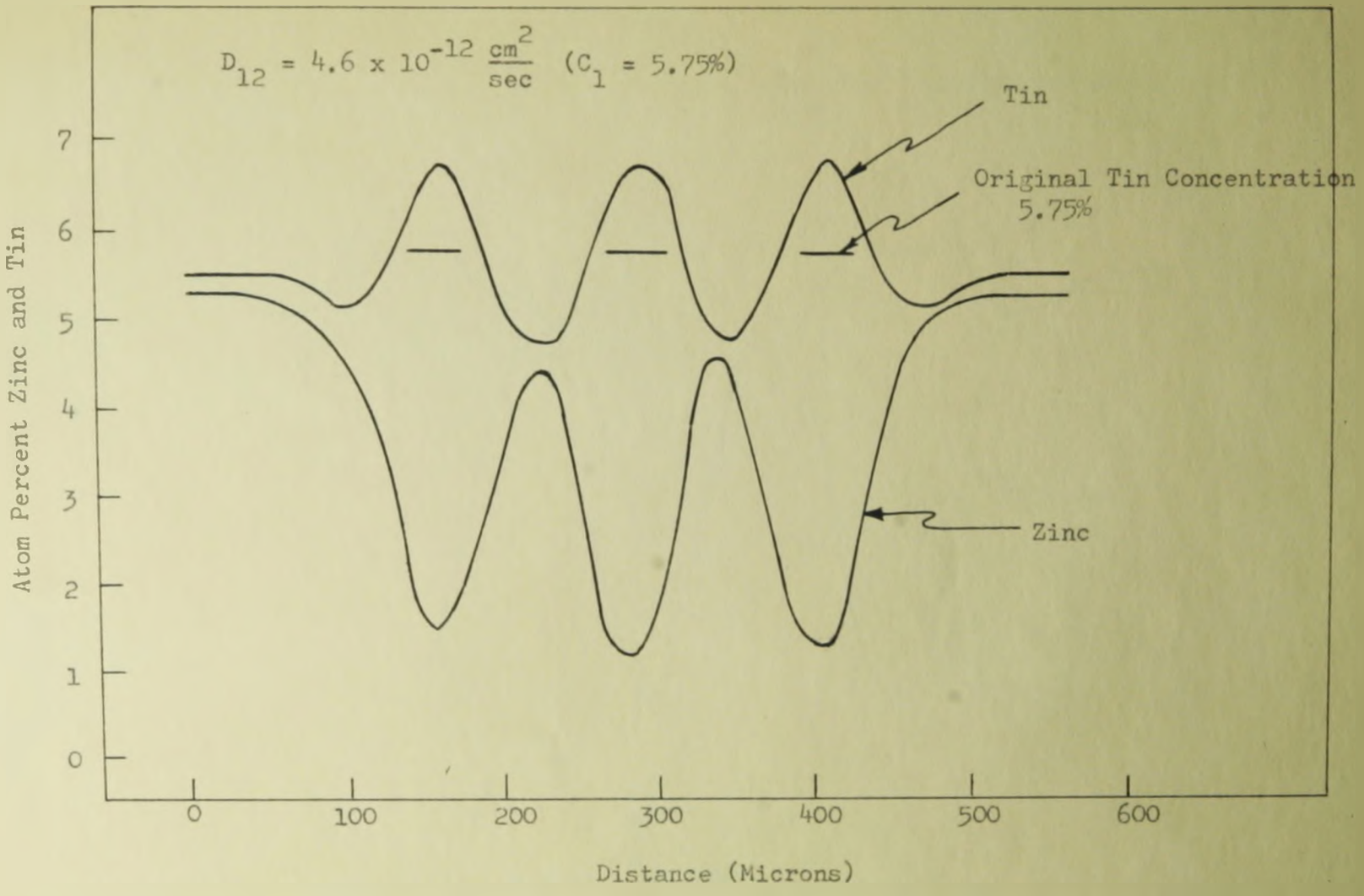

Figure 25 Concentration Profiles in Finite Cu Sn - Cu Zn Sn Couple

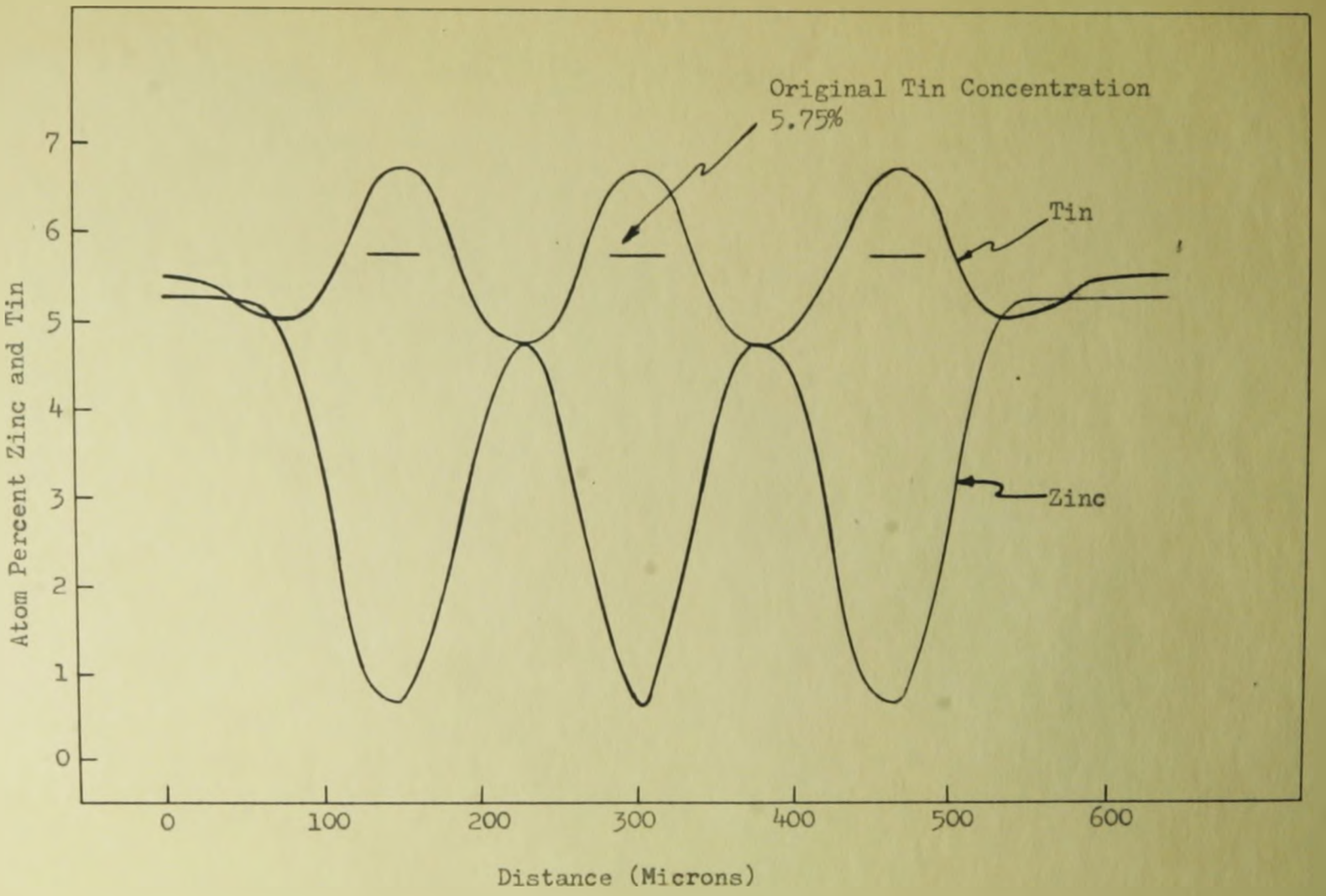

Figure 26 Concentration Profiles in Finite Cu Sn - Cu Zn Sn Couples

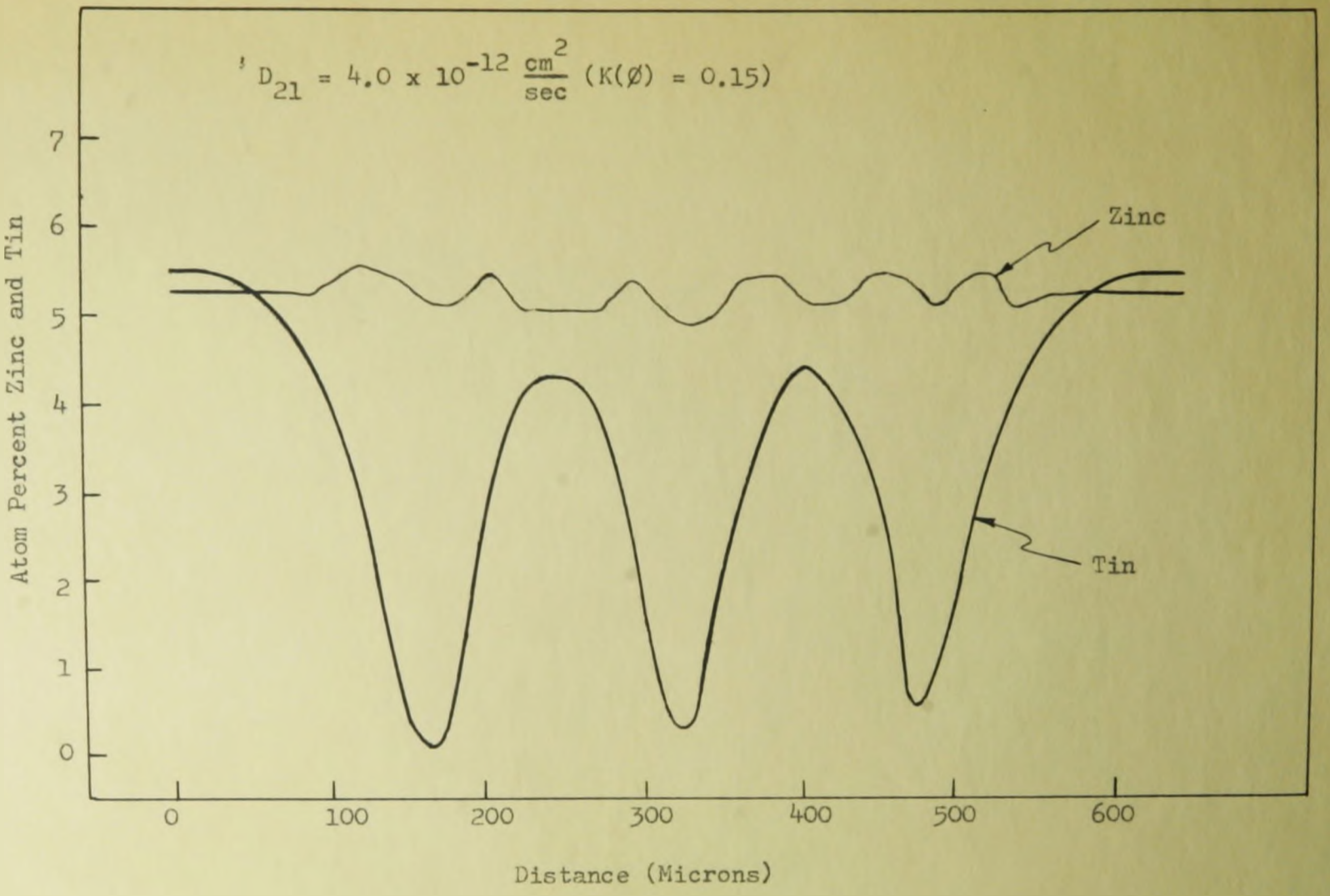

Figure 27 Concentration Profiles in Finite Cu Zn - Cu Zn Sn Couples

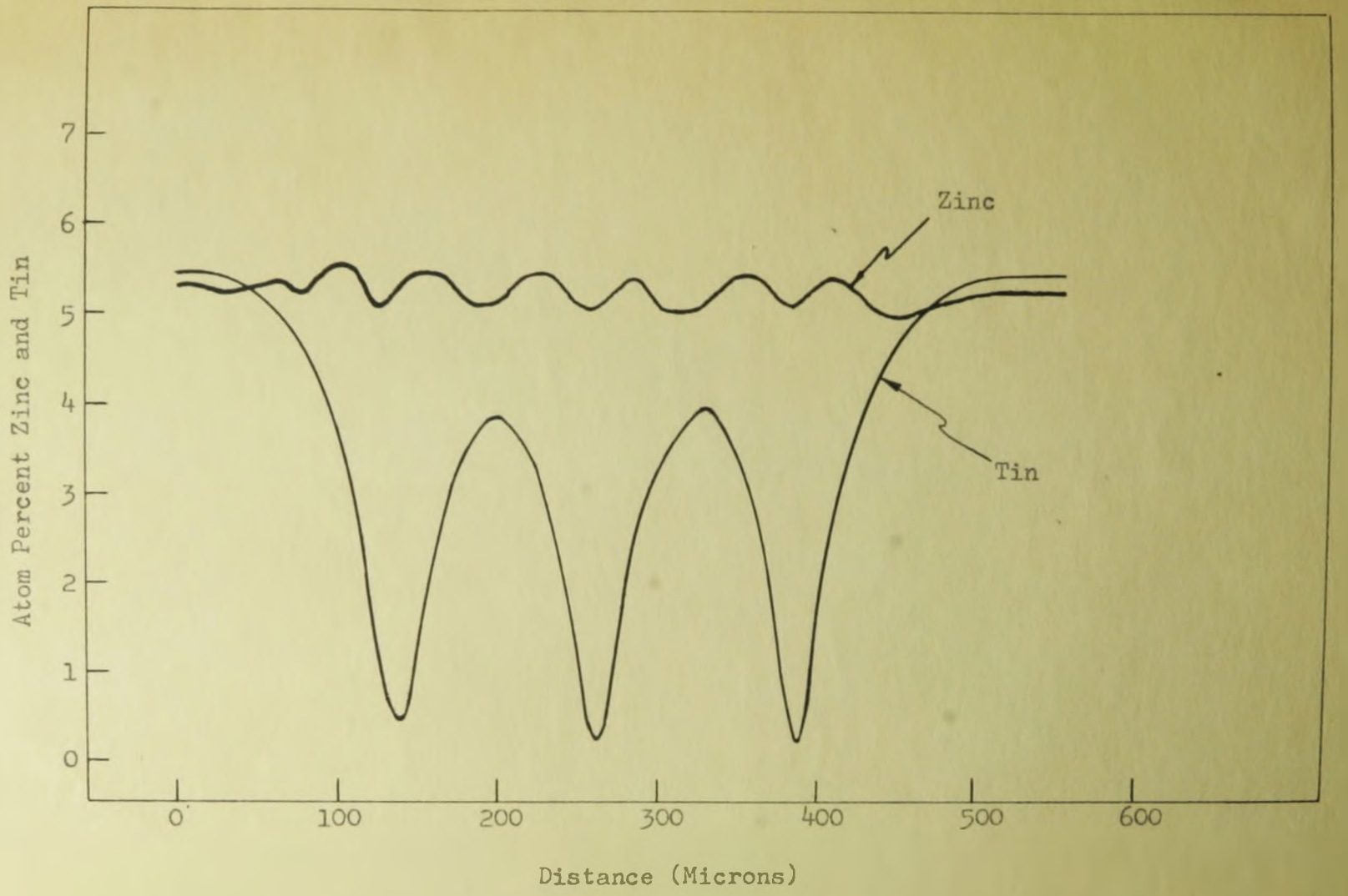

Figure 28 Concentration Profiles in Finite Cu Zn - Cu Zn Sn Couples